Tungsten Trioxide-based Variable Reflectivity Radiation Coatings for Optical Propulsion Applications

by

Joseph Niko Vlastos

A Thesis Presented in Partial Fulfillment
of the Requirements for the Degree
Master of Science

April 2020 by the
Graduate Supervisory Committee:

Liping Wang, Chair
Robert Wang
Ron Calhoun

ARIZONA STATE UNIVERSITY

May 2020

ABSTRACT

This thesis explores the potential application of the phase change material tungsten trioxide (WO_3) in optical force modulation for spacecraft and satellites. It starts with a literature review of past space optical force applications as well as potential phase change materials for optical force modulation. This is followed by the theoretical model and discussions of the optical properties of a variety of materials used in the structures explored thereafter. Four planar structures were analyzed in detail. Two of the structures were opaque and the other two were semi-transparent.

The first of the opaque structures was a tungsten trioxide film on aluminum substrate (WO_3/Al). It was found to have a 26% relative change in radiation pressure with WO_3 thickness of 200 nm. The second opaque structure was a tungsten trioxide film on silicon spacer on aluminum substrate (WO_3/Si/Al). This structure was found to have a 25% relative change in radiation pressure with 180 nm WO_3 and 20 nm Si.

The semitransparent structures were tungsten trioxide film on undoped silicone substrate (WO_3/Si), and a tungsten trioxide film on a silicone spacer on tungsten trioxide (WO_3/Si/WO_3). The WO_3/Si structure was found to have an 8% relative change in radiation pressure with 200 nm WO_3 and 50 nm Si. The WO_3/Si/WO_3 structure had a relative change in radiation pressure of 20% with 85 nm WO_3 and 90 nm Si.

These structures show promise for attitude control in future solar sailing space missions. The IKAROS mission proved the functionality of using phase change material in order to steer a space craft. This was accomplished with a 7.8% relative change in radiation pressure. However, this only occurred at a pressure change of 0.11 $\mu N/m^2$ over a range of 0.4

to 1.0 μm which is approximately 77.1% of the solar spectrum energy. The proposed structure (WO_3/Al) with a 26% relative change in radiation pressure with a pressure change of 1.4 $\mu N/m^2$ over a range 0.4 to 1.6 μm which is approximately 80% of the solar spectrum energy. The magnitude of radiation pressure variation in this study exceeds that used on the IKAROS, showing applicability for future mission.

ACKNOWLEDGMENTS

I would like to acknowledge and thank the following:

Fulton Underground Research Initiative (FURI) and ASU/NASA Space grant for funding my undergrad research projects and in doing so sparking my interest in a future in science and engineering.

Dr. Wang's lab (Nano-Engineered Thermal Radiation Group) which became mentors and friends. Professor Liping Wang for his dedication and mentorship over the past 3+ years. And Sidney Taylor for taking me under her wing. My Graduate Supervisory Committee: Liping Wang PhD, Chair, Robert Wang PhD, Ron Calhoun PhD. whose mentorship and guidance allowed my thesis experience to be positive and successful.

My friends throughout college with special thanks to Shaun Wootten for helping me get through my Biomedical Engineering undergraduate degree, Austin Kane for helping me get through Aerospace engineering, and Justin Givler MS whose support and lunch hours were the highlight of most weeks in graduate school. My amazing girlfriend Kirstin Peters whose brilliant mind astounds me on a daily basis, and whose company I hope to keep the rest of my life. With modesty and kindness she has helped me both academically and mentally through my entire academic career. Falling in love with her has been the most unexpected aspect of college and has taught me more about being human than a book will ever be able to.

My family for their constant unwavering support of all I do. My three siblings Zoe, Xander, and Kali Vlastos for being the examples of what the word sibling truly should mean, being there no matter what, thank you. My parents, Carrie S. Magill MD and Emanuel J. Vlastos MD, who have allowed me to explore my passions, support my dreams

in every way possible, truly being my biggest advocates, especially my mother, a medical doctor, health coach, yoga instructor, and so much more. The most amazing woman I have ever met has served as more than a typical mother, from confidant, friend and colleague she excels at it all. She has been my second pair of eyes, I depend on so much and use so often, yet she continues to give of her time and talent well beyond whatever the best mother would consider reasonable. My mother is and will continue to change the world and I will continue to strive to do the same. Thank you mom, you are truly the best.

TABLE OF CONTENTS

CHAPTER Page

CHAPTER 1

INTRODUCTION & BACKGROUND

1.1 Introduction

Fuel consumption for long duration space travel can be the limiting factor for interplanetary missions. This has been solved in the past by using radioisotopes. The spacecraft still are functioning today on Voyager 1 and 2 [1]. This is not the only way to reach interstellar space. Solar sailing is believed to be the most important future propulsion system in long duration space travel. This uses photons to push mass through space and thus needs no consumable fuel sources onboard. Although optical forces are very small the small acceleration over months and years adds up and can reach very high velocities. Solar sailing, a term used to depict pushing spacecraft through space using radiation pressure, has optimal performance with maximum optical force. By varying radiation pressure, the same phenomenon has been shown to be able to be used for steering a space spacecraft (attitude control). Attitude control was accomplished by the utilization of a phase change material that changes the reflectivity and thus changes the optical force being applied making the space craft steerable [2]. Vanadium dioxide (VO_2) and Polymer Dispersed Liquid Crystal (PDLC) has been analytically explored for this purpose in the past [3], [4].

In Fig. 1.1 the maximum torque possible is seen with the spacecraft on the right side, which is varying from transmission to reflectance, whereas the spacecraft on the left is varying between absorption and reflection. This is in part due to reflection causing the largest radiation pressure P_1, followed by absorption P_2, and almost no radiation pressure with transmission P_2. Thus, simply put $P_2 > P_1 > P_3$. Resulting in that $(P_2 - P_1) <$

$(P_2 - P_3)$. Meaning that the spaceship on the right will have a greater torque and thus ability to control trajectory.

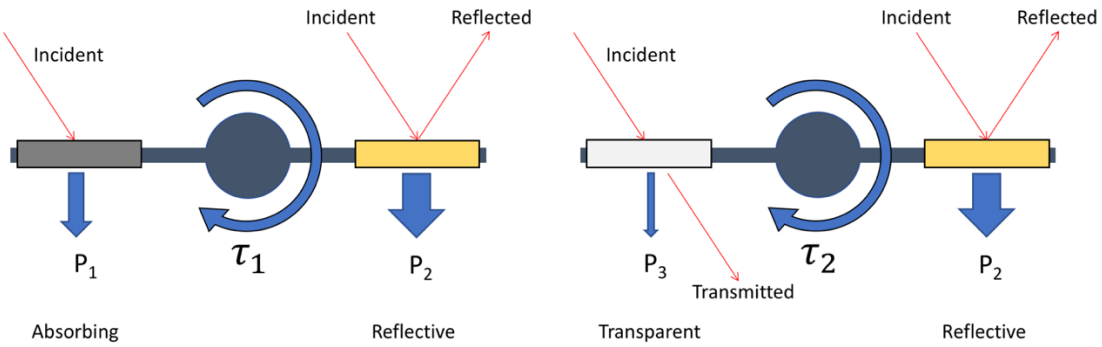

Figure 1.1: Schematic of a solar sailing spacecraft from the side. Solar sails are off to the side whereas the modulating portions are gray, yellow and white rectangles. Yellow rectangles represent perfect reflectivity using the greatest pressure P_2. The gray rectangle is absorbing and has radiation pressure P_1. The white rectangle is transparent with a very small radiation pressure P_3. τ_1 and τ_2 denotes the torque caused by the different optical pressures on the two sides of each space craft.

1.2 Background on Space Applications of Radiation Pressure

One of the primary space applications for optical force caused by radiation pressure is the solar sail. Solar sail functions by utilizing the radiation from the sun to propel the spacecraft through space. The mechanisms for which this occurs are photons absorbing into whatever craft is being pushed through space or reflecting off of it. The change in momentum of these particles endows a small force that can be utilized to propel a spacecraft. Past applications of this phenomenon are explored here.

Funase et al. [2] working with Japan's NASA equivalent, JAXA developed a solar sail named the IKAROS (Interplanetary Kite-craft Accelerated by Radiation Of the Sun). This was a spinning type of solar sail. The spinning type solar sail uses rotational acceleration as the force to hold it in an extended position. The other kind is the rigid type

solar sail. This is something that has a rigid skeleton that holds the solar sail open. The JAXA's IKAROS Mission was a spin type solar sail, which utilized a phase change material switched from diffuse reflection to specular reflection. Funase et al. [2] show that the diffuse reflection is 2/3 of the specular reflection under the same conditions contributing to radiation pressure. This in a physical sense is due to diffuse reflection perpendicular components not contributing to the pressure in the direction of the beam. As a consequence, the amount of optical pressure felt by the solar sails would be changed. This subsequently allowed them to steer this solar sail using a control system that would electrically change the reflectivity of the material. It is well known that the diffuse reflectivity will produce less force and spectral reflectivity. This can be shown through theoretical equations and will be done later in this paper. This paper goes on to explain how using solar radiation pressure imbalances created by electrical charges changing the phase change material on the outer edge of the rotating solar sail allows the ability to maneuver the solar sail in space. The maneuverability of the solar sail is done without any oscillations, which is one of the main concerns with using conventional boosters on the body of the spacecraft. This then allows the solar sail to eliminate the oscillations as one of the biggest limiting factors previously.

Ma et al. [5] used liquid crystal films which switch between the transmissive on state and the opaque off state. They claimed that using these liquid crystals, it was able to outperform the IKAROS Mission by a factor of four. This showed a 53% change in radiation pressure with a modulation of 0.5 $\mu N/m^2$. This outperformed IKAROS that had a 7.8 % change in radiation pressure with a 0.11 $\mu N/m^2$. This work only calculated over the range of 400–1100 nm for the solar spectrum. Theoretically the difference in optical

pressure between perfectly transmissive would have an optical pressure of zero. Changing to opaque typically means it is absorbing or reflecting all of the energy. This will have a greater pressure difference than the previous two: diffuse reflectivity and spectral reflectivity. In this paper he derives these optical properties to calculate from pressure differences from first principles.

Taylor et al. [6] published a conference paper focused on optical force space application of vanadium dioxide (VO_2), a phase change material that changes from an insulator to metal at a temperature of 341 K. Below this temperature VO_2 is dielectric and above this temperature it is a metal. This paper went into a theoretical design for a space application of the phase change structure, which utilized a Fábry Perot cavity as well as an anti-reflective surface on the top. A gold layer was considered as the top of the Fábry Perot cavity, vanadium dioxide (VO_2) was used as the middle dielectric layer depending on the temperature, and a thick tungsten bottom layer was used as a mirror. This succeeded in producing a 20% change in optical force between the insulator-to-metal states and a radiation pressure change of 1.8 $\mu N/m^2$.

Some materials show significant promise in optical force applications such as niobium pentoxide (Nb_2O_5). The literature indicates that this material both switches states thermochromically and electrochromically. There are many studies on this material as well as different applications. The level of switching is enough to be a promising material to explore further and thus is listed here. However, as research was conducted the realization that a comprehensive set of data in both transition states has not been recorded in the literature to our knowledge to date.

Tungsten trioxide (WO_3) has not as of yet been fully explored in optical force applications. However due to its electrochromic property that allows it to change from a dark to a light material by changing its optical properties in the presence of an electric potential, tungsten trioxide has been explored for application in smart windows. One paper describes the necessary circumstances to see an electrochromic behavior occur. Electrochromic is more than just a monolayer of WO_3 it is several layers one of which is WO_3 and typically referred to as the active layer. To elicit a response in WO_3 two particles need to be inserted into the lattice structure. First a positive ion such as Li^+ and H^+ and second an electron to balance out the charges. Both the cation and electron will migrate into the lattice structure of WO_3 changing its structure when electrical potential is applied [7]. There are several architectures that have been used in smart window applications. It is believed that this phenomenon can be taken advantage of for optical force applications and to achieve comparable or better performance than those with vanadium dioxide (VO_2) and polymer dispersed liquid crystal (PDLC).

1.3 Background on Potential Phase Change Materials

There is a significant body of research on vanadium dioxide. The optical properties are measured and fit with models. Some of the seminal work in this area was first done by Barker et al 1966 [8] where he measured the optical properties of vanadium dioxide in the infrared range that is between 100 to 20000 cm^{-1}. This corresponds to 100.00 μm to 0.50 μm. The properties were calculated both above and below the transition temperature of vanadium dioxide which is at 341 K. This same group published the second paper VERLEUR et al 1968 [9] where they focused on the visible range between 0.25 and 5

electron volts which corresponds to 4.96 μm to 0.25 μm. They also measured optical properties of vanadium dioxide above and below the transition temperature. They briefly discussed the physical lattice change in vanadium dioxide that results in a property change from a semiconductor to a metal. This gives us an experimentally derived model of vanadium dioxide through the infrared and visible range.

Taylor, et al. 2019 [6] explore the extraction of optical properties from vanadium dioxide, verifying the pureness of VO2. In X-ray diffraction they found that between the two phases there was a 57% change at the wavelength of $\lambda = 2.5$ μm as well as a 7% change in transmittance over the entire visible spectrum. They also experimentally found that the phase changes over in the 20 K range from 345 K to 325 K.

Polymer Dispersed Liquid Crystal (PDLC) Ma et al. 2016 [6] has been explored here for their solar sailing applications. This was a ground-based study that used the IKAROS Mission as a benchmark to beat. PDLC has the ability to switch from transparent and scattering states, which greatly changes the optical pressure output and they claimed they would outperform the IKAROS Mission by more than four times. This was done using the ability of liquid crystals to switch from an opaque to a transparent material with only the application of an external electric field. In this study the external electric field applied to their samples was 100 V. The way that PDLC films function is that they consist of liquid crystal microdroplets that are mixed with the polymer matrix. This results in crystals that are polarized with a positive and negative portion and will align when the electric field is applied. The crystal becomes clear when the external electric field is applied. When the crystals are randomly dispersed, they appear opaque. The heat transfer significance of this

is that no heat transfer occurs if a material is perfectly transmitting. The heat transfer is much greater if the surface is opaque. PDLC has great potential in optical force application.

Niobium pentoxide Nb_2O_5 is a material that shows great promise as a phase change material that may be well suited for control of optical force. However, after a literature review further studies on optical properties at both its states are needed before analytical analysis of its use in such application can take place. Brief review of niobium pentoxide Nb_2O_5 is as follows.

Braga, V. S., et al 2018 Explored niobium pentoxide on silica -alumina Nb_2O_5 /SiO_2 Al_2O_3 This used a variety of imaging techniques to look at the four different types of crystalline structure found in niobium pentoxide. These crystalline structures are hexagonal (TT) orthorhombic (t or upsilon) , Monoclinic(M of Bate), and monoclinic (H or alpha). The Nb_2O_5 weight changes upon heating. An analysis of temperature increases in the sample Nb_2O_5 /SiO_2 Al_2O_3 With increasing percent mass of niobium pentoxide, results found that there was a phase change at around 1364°C. Further results indicated that predominately orthorhombic (T) and monoclinic (H and M) were observed with doped Nb_2O_5 which contrasts with pure Nb_2O_5 which would result in monoclinic phase (H) under the same conditions [10].

Chudnovskii, F A, et al. 1996. explored oxides of transition metals including Nb and V both of which are of interest in controllable reflectivity of surfaces. This paper was looking at the phenomenon of S shaped resistance curve on an I – V diagram. This is presumably caused by the phase of the material as it changes from one phase to another due to heating and or voltage running across the material. The results showed that they quantify that there was some temperature T_o that if above there was no switching observed.

This is because the material has already transitioned to a metal from an insulator. This temperature was different in each transition metal 120 K for Fe3O4, 340 K for VO_2, 500 K for Ti_2O_3, and 1070 K for NbO_2. Proving that NbO_2 as well as other materials phase transition with current application as well as increased temperature [11].

Emmenegger, & Robinson in 1968 goes over the dielectric properties in different crystal states calculating the dielectric constant and reflective index. However, this paper only focuses on very large wavelengths between 2 and 100 MHz. These numbers roughly estimate 15m to 2m which are very large wavelengths close to radio frequencies. Thus, these optical constants are unlikely to be accurate for the visible and near infrared region of the electromagnetic scale [12].

As with many phase change materials in recent years they have been explored for their uses in smart windows. Niobium is no exception to this rule and was explored by many researchers including Ulrich, Stephan, et al 2016 [13] with titanium niobium mixed oxide films. The transmitted and reflections of these doped niobiums found a large change in these properties with the application of both negative and positive voltage across the layered material made [13].

The electrochromic properties of tantalum pentoxide doped niobium pentoxide are explored here. Most importantly they also had a 0% doped sample meaning it was pure niobium pentoxide. This would allow the optical properties to be pulled out of this for niobium [14]. The data provided is all below the transitional temperature, and none is provided above the transition temperature. This prevents the use of these properties to explore optical force modulation. This information can also be found on the website: refractiveindex.info [15].

Literature review of tungsten trioxide, WO_3 provides good insight into how to make an electrochromic layer change states. Jaing et al. [16] published this paper focusing on investigating optical constants of WO_3, NiO, and Ta_2O_5 thin films. The thin films prepared by electron beam evaporation and measured using spectroscopic ellipsometry showed results agreeing with the calculated optical properties.

An electrochromic material was explored in a TC/EC1/IC/EC2/TC. Where each of these are a layer such that TC = transparent electrical conductor, EC1 and EC2 are the electrochromic layers, and IC is the ion conductor. The EC1 and EC2 can be the electrochromic materials that may or may not store ions. Bypassing voltage crossed EC1 and EC2 causing ions to move from EC1 through IC to EC2 or vice versa depending on the direction of voltage. This changes the transmittance of the electrochromic device. By adding an electric current one can change the optical properties of the device.

WO_3 and NiO were used as the EC1 and EC2 electrochromic layers. The IC was tantalum pentoxide (Ta_2O_5). The lower layer of TC was a reflective layer of aluminum AL and the top TC layer was a transparent conductive indium tin oxide (ITO) film [16]. ViolBarbosa et al 2016 [17] focused on the electrochromic properties of tungsten trioxide, WO_3. There was a short discussion of ways to manipulate WO_3 properties by doping it with electro positive elements such as Rb, K or Cs, and H which can result in converting this insulator into a metallic conductor or even a superconductor. WO_3 transmitted can also be manipulated by adding cations such as H^+ or Li^+. This paper goes on to explain and explore a way of liquid electrolyte gating. Ionic liquid gating has been shown to suppress the metallic to insulator transition. Ionic liquid gating has been shown to cause structural changes in VO_2. This paper goes over the structural changes found in WO_3 with the

modification of the energy bands. This can result in a transparent conducting oxide. To accomplish this a process of placing a droplet of 1-hexyl-3-methylimidazolium bis(trifluoromethylsulfonyl)- imide (HMIM-TFSI) directly on the surface of WO_3. The voltage of 3 V was applied across the surface for 10 hours. Then this liquid was cleaned off the surface and measurements were taken. The measurements were taken before, right after, and then a significant time after the liquid gating took place. Results found that the electric gating process resulted in a crystalline structure that weakened the oxygen bonds of WO_3. This allows the favoring of weakened covalently bonded oxygen and trapped non-bonded oxygen. The authors suggest that phenomenon of tendencies towards metallic behavior is caused by electronic transfer from weakly bonded oxygen to new in-gap states. This causes an overlap with the bottom of the conduction band resulting in the metallic behavior. These restrictions cause absorption outside the visible range, making this a potential. In the paper written by ViolBarbosa et al. (2016) [17] they produced their samples in the following way. Laser deposition was used to grow epitaxial WO_3 single-crystalline films in a $LaAlO_3$ substrate. A laser running a pulse rate of 4 Hz and with an energy density of ~0.7 J cm^{-2} and 7.1cm from the polycrystalline WO_3 was targeted at 750 °C ViolBarbosa et al. (2016) Supporting Information [17]. To expand this process pulsed laser deposition will be explored in more detail here.

Pulsed laser deposition is a simple method in which a high-power laser beam is directed into a vacuum chamber and is incident on the material that one would like to create a thin film. The instant laser energy is converted and creates a plasma plume. This thin deposit on the substrate is typically held above the target material that the laser is hitting.

This well-known technique creates simplicity and versatility in creating thin films of a vast array of materials and has made it popular today with multilayered structures [18].

Piccolo et al 2015 and 2016 published two papers; the second expanding upon the first, on the performance possibilities of smart window glazing. Some of the performances analyzed were switching voltage, switching speed, optical memory, optical transmittance coefficient, source keychain, reflecting coefficient, and thermal transmittance. This paper discussed low energy western facing voltage draws of large window devices that also have an optical memory defined here. After voltage is applied to change the optical properties, the device will remain at that changed state for extended periods of time, here greater than 10 hours. This produces the energy needs to the device in question. Architecture for the smart window device was Glass/SnO_2:F/WO_3/PEO:Li/NiOH:Li/SnO_2:F/Glass.

The layers start with the active layer which is tungsten trioxide which was sputtered coated on. The ion storage layer is a nickel hydroxide film electronically deposited and then treated by insertion of lithium ions by cyclization in a saturated LiOH 1 N electrolytic solution. The layer between the two is a polymeric electrolyte which also uses lithium that is dissolved. This whole device is sandwiched by transparent conductive layers that function as the two voltage terminals the cathode and anode.

The ion storage layer and the active layer have electrochromism properties that complement each other. As the voltage is passed through the multilayered structure with a negative electron moving in to the active layer, this side is called the working side or cathode and the NiOH:Li is known as the anode. This voltage causes cations to move through the ion conductor and into the active material, here tungsten trioxide changing the optical properties. Consequently, tungsten trioxide as well as nickel oxide complement

each other meaning that as one bleaches so does the other. This effect can be reversed by reversing the voltage. This paper shows that the optical memory (after voltage is applied how long the material's optical changes last) is greater than 10 hours. This architecture shows great promise for smart window devices and may also serve for other optical coding in the future [19], [20].

After substantial literature review it was found that there was no suitable data set available for both states of niobium pentoxide Nb_2O_5. In further chapters Nb_2O_5 is not explored further due to a lack of data to use it in the mathematical models used. Fortunately, tungsten trioxide's, WO_3 literature review resulted in data sets. Each of these data sets included data for both states before and after transition. The first data set was from Jaing et al 2013 [16] and was over the wavelength of 0.4 μm to 0.7 μm. This is essentially the visible range of the electromagnetic spectrum and does not contain the majority of solar radiation. The second data set by ViolBarbosa et a. (2016) [17] was obtained which went from 0.4 μm to 1.6 μm. This range contains roughly 80% of the solar energy. In subsequent mathematical models ViolBarbosa's data for tungsten trioxide, WO_3 is used.

1.4 Objectives

Tungsten trioxide (WO_3) is an electrochromic transition metal that has a phase with the application of electrical voltage. This is changed by injection of positive ions such as Li^+ and H^+ and an electron to balance the charge into the host material, i.e., WO_3. This migration changes the lattice structure significantly enough to change the optical properties to be lightening or darkening. This makes WO_3 a good candidate for tunable radiation coating that will allow control of optical force applied to a spacecraft [7]. Phase change properties of WO_3

have been taken advantage of by many smart window applications. However, to date there has been no literature on using WO_3 radiation pressure or optical force applications. It is this gap in optical force of WO_3 literature that this paper hopes to fill.

This thesis plans to do the systematic approach to this end, starting with a brief literature review in chapter 1, followed by a discussion in chapter 2 of materials optical properties *n* and *k*, and the theory to model the radiative properties of thin-film structures. Chapters 3 and 4 will be an exploration of material structures layering of different materials in order to achieve the greatest change in optical force between the gated (bleached) state and the ungated (colored) state. This exploration takes a step-by-step approach, first looking at a single layer of tungsten trioxide, followed by a WO_3 thin film deposited on either aluminum as an opaque surface or silicon as a semitransparent surface. The last is a tri-layered structure: tungsten trioxide, then silicon as the middle layer on an aluminum base layer (WO_3/Si/Al), or tungsten trioxide, then silicon as the middle layer and tungsten trioxide as the base layer (WO_3/Si/WO_3). Both of these two utilize a Fábry-Perot cavity increasing reflectivity in one of these states.

A Fabry-Perot cavity is one of the architectures explored in the chapters to come. Fabry-Perot cavities consist of a thin metallic layer followed by a dielectric material, followed by a thick metallic layer. Incident electromagnetic waves at certain frequencies will get trapped between the two metallic surfaces thus increasing the absorption of those wavelengths. In addition to the Fabry Perot cavity there is also several layered structures that will be explored throughout this paper. Regardless of the architecture, the analysis will use a similar approach.

These optical properties of each material in a multilayered sample will be used to simulate the optical force created by electromagnetic waves in the visible and infrared spectra. This will then be used to maximize the difference in optical force between the bleached and colored states. By maximizing the pressure differences, one allows the spacecraft to have the most maneuverability.

In order to maximize the change seen in the Fábry Perot cavity, WO_3 is utilized as either the upper layer or both the upper and lower mirrors. WO_3 is capable of changing from the typical "colored" absorbing state to a semitransparent "bleached" state by applying voltage across WO_3. In order to apply this full voltage and thus have the change in optical effect several very thin layers are necessary of transparent conductors, ion conductive layer and the ion storage layer. These associated layers are not taken into account in the optical model presented here.

CHAPTER 2

OPTICAL PROPERTIES & THEORY

Chapter 2 goes over the theory behind radiation pressure and optical force starting in Section 2.1 with a derivation of the radiative pressure equation in terms of q_r and q_{abs}, reflection and absorption respectively. Section 2.2 briefly describes the optical properties used in this system as well as where they were obtained from. Section 2.3 briefly goes over how to calculate reflection and absorption from the optical properties themselves at a single interface between two semi-infinite materials. Then section 2.4 goes into depth on how to theoretically model the spectral radiative properties for multilayer thin film structures.

2.1 Radiation Pressure Calculation

First, we have to go back to electromagnetic wave theory: in addition to being viewed as a wave, the electromagnetic spectrum can also be viewed as a particle which has a certain speed and a certain energy associated with it. Viewing this particle to have energy and velocity, it is then possible to calculate the momentum it has as a particle. Based on Einstein's equation $E = Mc^2$, we can find its theoretical mass for this thought experiment. Three scenarios are explored in absorption, reflection and transmission.

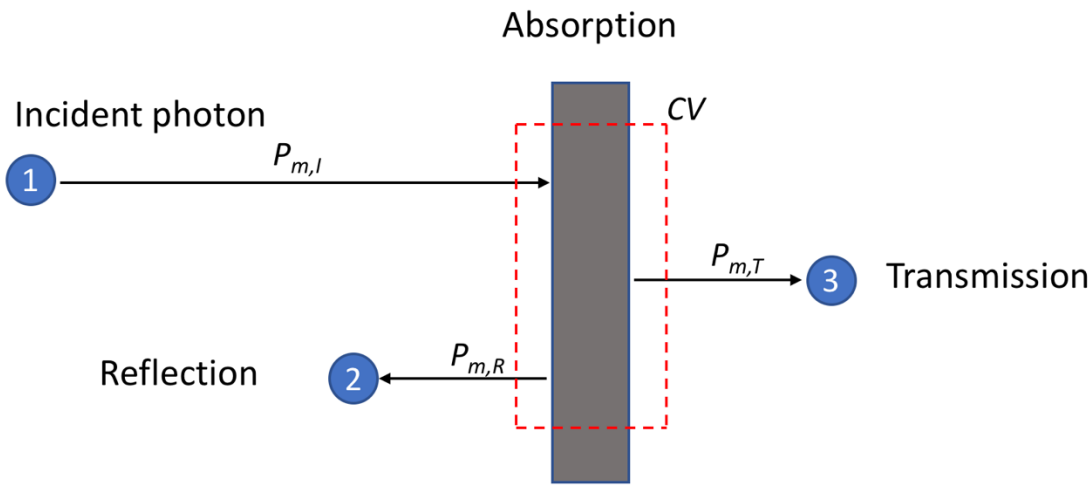

Figure 2.1: An incident photon (1) is shown hitting thin film, which will either be reflected (2) or transmitted (3) or absorbed not shown since it does not leave the control volume (CV). $P_{m,i,}$ $P_{m,R}$ and $P_{m,T}$ are the momentum of the incident, reflected and transmitted photons respectively.

Taking the momentum balance of Figure 2.1we see that we achieve the total momentum to be equation 2.1.2.

$$p_{m,tot} = p_{m,I} + p_{m,R} - p_{m,T} \tag{2.1.2}$$

In equation 2.1.2 $p_{m,I}$ represents the momentum transferred to the control volume by the incident photon (1). $p_{m,R}$ represents the momentum added to the control volume of a photon leaving by reflection (2). $p_{m,R}$ represents the momentum lost from the control volume of a photon leaving by transmission (3). This is assuming momentum is defined as positive to the right-hand side. Knowing that $p_{m,I} = p_{m,R} + p_{m,T} + p_{m,A}$ then it can be rearranged to $p_{m,I} - p_{m,T} = p_{m,R} + p_{m,A}$ and thus can be plugged in to equation 2.1.2 simplifying it to equation 2.1.3.

$$p_{m,tot} = p_{m,R} + p_{m,R} + p_{m,A} = 2p_{m,R} + p_{m,A} \tag{2.1.2}$$

Another equation for momentum: Force times change in time equals momentum, seen in this equation 2.1.3.

$$p_m = F \times \Delta t \tag{2.1.3}$$

In this equation, F represents force, Δt represents change in time. We also know that Energy equals force over a distance equation 2.1.4.

$$\Delta E = F \times \Delta x \tag{2.1.4}$$

In this equation Δx represents the change in distance. Solve an equation 2.1.4 for Force $F = \Delta E/\Delta x$ and plugging this into the equation 2.1.3 we get equation 2.1.5.

$$p_m = \frac{\Delta E}{\Delta x} \times \Delta t = \frac{\Delta E}{\frac{\Delta x}{\Delta t}} \tag{2.1.5}$$

It is then possible to substitute velocity for $\frac{\Delta x}{\Delta t}$ which is of course the speed of light. So, we will replace it with the speed of light C. This then gives equation 2.1.6.

$$p_m = \frac{\Delta E}{C} \tag{2.1.6}$$

Thus, the momentum of an absorbed electromagnetic beam in terms of known values. The radiation pressure form absorption is found next. Starting from the most basic equation for pressure which is equation 2.1.7. Where P_p is the pressure and A is the area.

$$P_p = \frac{F}{A} \tag{2.1.7}$$

Rearranging equation 2.1.2, $F = P_m/\Delta t$ and plugging into equation 2.1.7, equation 2.1.8 is achieved.

$$P_p = \frac{p_m}{\Delta t}\frac{1}{A} \tag{2.1.8}$$

Plugging in for change in momentum, using equation 2.1.6 results in refined equation 2.1.9.

$$P_p = \frac{\Delta E}{\Delta t}\frac{1}{AC} \tag{2.1.9}$$

Pulling out $\frac{\Delta E}{\Delta t}$ from equation 2.1.9 it is seen that this is equivalent to Q_{rad}, radiative heat transfer. This leads to $\frac{\Delta E}{\Delta t}\frac{1}{A} = \frac{Q_{rad}}{A} = q_{rad}$ where q_{rad} is basically radiative heat flux with units of [W/m^2]. Furthermore $G = q_{rad}$ where G is solar irradiance and is equal to radiative heat flux in [W/m^2]. Thus equation 2.1.9 can be rewrote as $P_{p,A} = q_{rad}\frac{1}{C}$ then rearranging equation 2.1.6 and plugging it in to equation 2.1.9 we get equation 2.1.10.

$$P_p = \frac{1}{C}\left(\frac{\Delta E}{A\,\Delta t}\right) = \frac{1}{C}\left(\frac{p_m \times C}{A\,\Delta t}\right) = \frac{1}{C}q_{rad} \tag{2.1.10}$$

And finally plugging in the momentum balance, equation 2.1.2 into equation 2.1.10 it is found that each component of momentum, reflection and absorption can be converted to its associated heat flux, equation 2.1.11.

$$P_p = \frac{1}{C}\left(\frac{2p_{m,r} \times C + p_{m,abs} \times C}{A \times \Delta t}\right) = \frac{1}{C}\left(2\left(\frac{p_{m,r} \times C}{A\,\Delta t}\right) + \left(\frac{p_{m,abs} \times C}{A\,\Delta t}\right)\right) \tag{2.1.11a}$$

$$P_p = \frac{1}{C}(2q_r + q_{abs}) \tag{2.1.11b}$$

then substituting $q_{abs} = \alpha \times q_{rad}$ and $q_r = \rho \times q_{rad}$ where $q_{rad}$is the radiative heat flux on the surface and α and ρ are the absorptivity and reflectivity equation 2.1.12 is found [21].

$$P_p = \frac{1}{C}q_{rad}(2\rho + \alpha) \tag{2.1.12}$$

Material with a reflectivity of ρ and an absorptivity α could simply be represented by the q_{rad}. We did not realize that we are calculating the simple list form of this equation having an incidence of zero and a view angle equaling to one, and for a single wavelength. It would follow that finding the total hemispheric reflectivity, and total hemispheric absorptivity would make equation 2.1.12 useful. The equation for the total hemispheric

reflectivity is equation 2.1.13 and 2.1.14, respectively total hemispheric reflectivity and total hemispheric absorptivity [21].

$$\rho = \frac{\int_0^\infty \rho_\lambda \int_{2\pi} I_\lambda \cos(\theta) \mathrm{d}\Omega d\lambda}{\int_0^\infty \int_{2\pi} I_\lambda \cos(\theta) \mathrm{d}\Omega d\lambda} \tag{2.1.13}$$

$$\alpha = \frac{\int_0^\infty \int_{2\pi} \alpha'_\lambda I_\lambda \cos(\theta) \mathrm{d}\Omega d\lambda}{\int_0^\infty \int_{2\pi} I_\lambda \cos(\theta) \mathrm{d}\Omega d\lambda} \tag{2.1.14}$$

Equation 2.1.13 for total hemispheric reflectivity ρ_λ represents the spectral reflectivity, the reflectivity at each wave. In both equation 2.1.13 and 2.1.14 I_λ represents the solar intensity which is closely related to radiative heat flux and is for each wavelength individual and therefore the units are [W/m2/Sr] for solar intensity I_λ. The $\cos(\theta)$ is the direction of the incoming radiation. dΩ is the view angle. In equation 2.1.14 α'_λ is the spectral directional absorptance.

2.2 Optical Properties

Throughout the exploration of modulating optical force, many structures will be explored and will be expanded upon in future chapters. Here optical properties of each material used in these structures are presented. The n and k are both presented for each material. Furthermore, if this material changes state, both the states are shown on one n and k graph. Optical properties are the core of each material and being able to view their properties versus wavelength allows a more comprehensive understanding of how they may interact and be used in future architectures.

Although some of the optical properties are found utilizing extracted data from past experiments and inputting the oscillators for either the Drude model, Lorentz model or a combination of the two, the vast majority are collected directly from the data provided and

past papers, and use a simple interpolation scheme to find the continuation of each line. The *n* and *k* graphs of materials used in this study are shown here.

Following is an important equation to be familiar with relating the optical properties in the previous section *n* and *k* to that of the permittivity used in many models to come. Equation 2.2.2 is exactly such an equation [21].

$$\varepsilon = (n + ik)^2 \tag{2.2.2}$$

In Equation 2.2.2 permittivity is noted by ε. It is noted that i is an imaginary number. Thus, we find the complex permittivity which becomes very useful in models to come. This serves as a very quick overview to better understand what n and k represent on each graph.

The next three graphs depict the refractive index (n) and the absorptive index (k) for aluminum (Al), silicone (Si) and tungsten trioxide (WO_3).

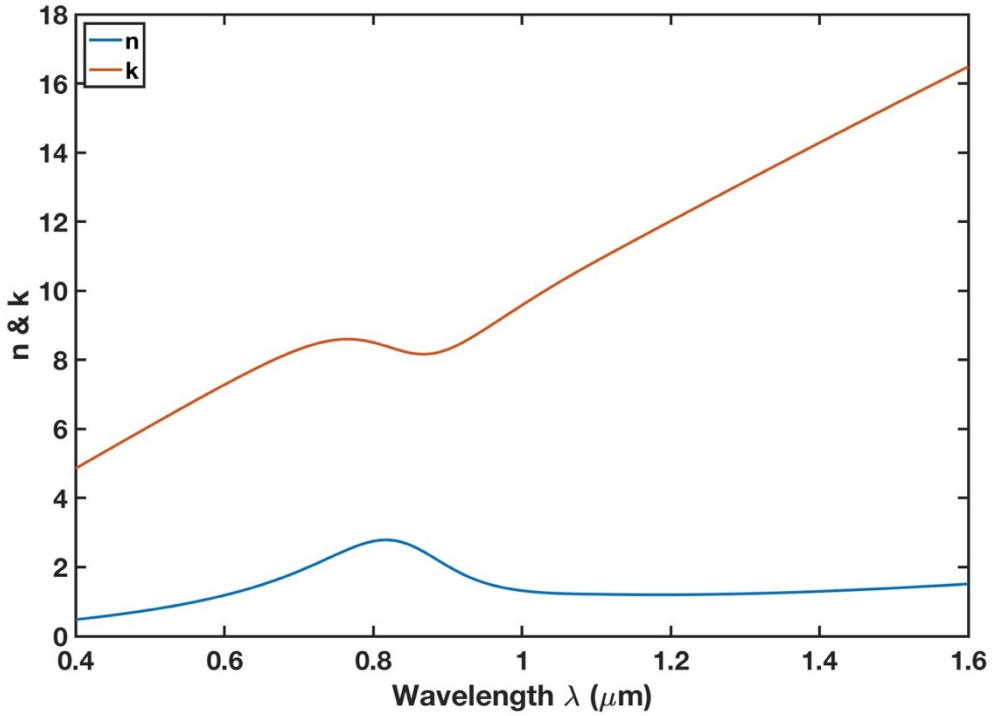

Figure 2.2: Aluminum (Al) refractive index (n) and absorptive index (k) over wavelengths 0.4 to 1.6 µm. Refractive index (n) solid blue line, absorptive index (k) solid red line [22].

Aluminum has a relatively high reflective index. At 0.4 µm it is approximately 5 and this continues upward consistently so that by 1.6 µm n is above 16. Aluminum is very reflective especially at higher wavelengths. Absorptive index is consistently increasing until around 0.82 µm where there is a relative maximum. After this maximum the *k* declines until 1.1 µm then inclines slowly to 1.6 µm.

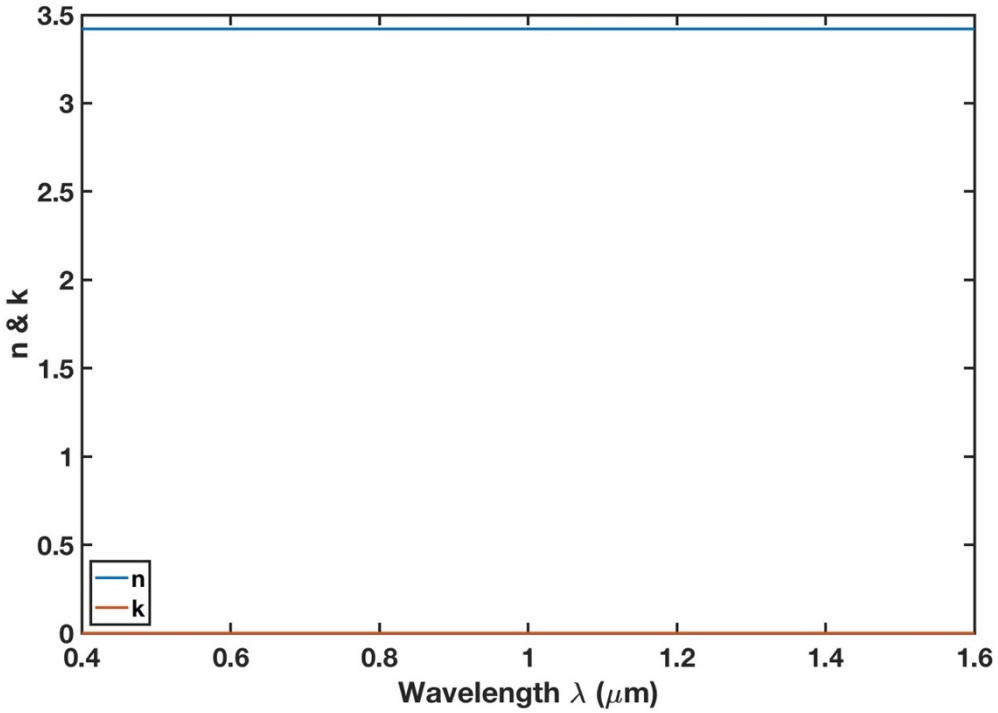

Figure 2.3: Silicone (Si) refractive index (n) and absorptive index (k) over wavelengths 0.4 to 1.6 µm. Refractive index (n) solid blue line, absorptive index (k) solid red line [23].

Silicone's reflective index is almost constant across the spectrum, observed here from 0.4 µm micrometers to 1.6 µm. But the reflective index of roughly 3.5 is the reflectivity and is not great and thus is considered to be semitransparent. Absorption index is also important and plays a key role in equation 2.2.7 for transmissions through a material.

$$\tau = e^{-4\pi k_2/\lambda} \tag{2.2.7}$$

In equation 2.2.7 absorptive index is k and λ is the wavelength of incident light. This shows that the absorption index increases as the transmission decreases and thus the absorption must increase. Thus, it becomes apparent that silicone absorbs very little and therefore has a very small absorption index

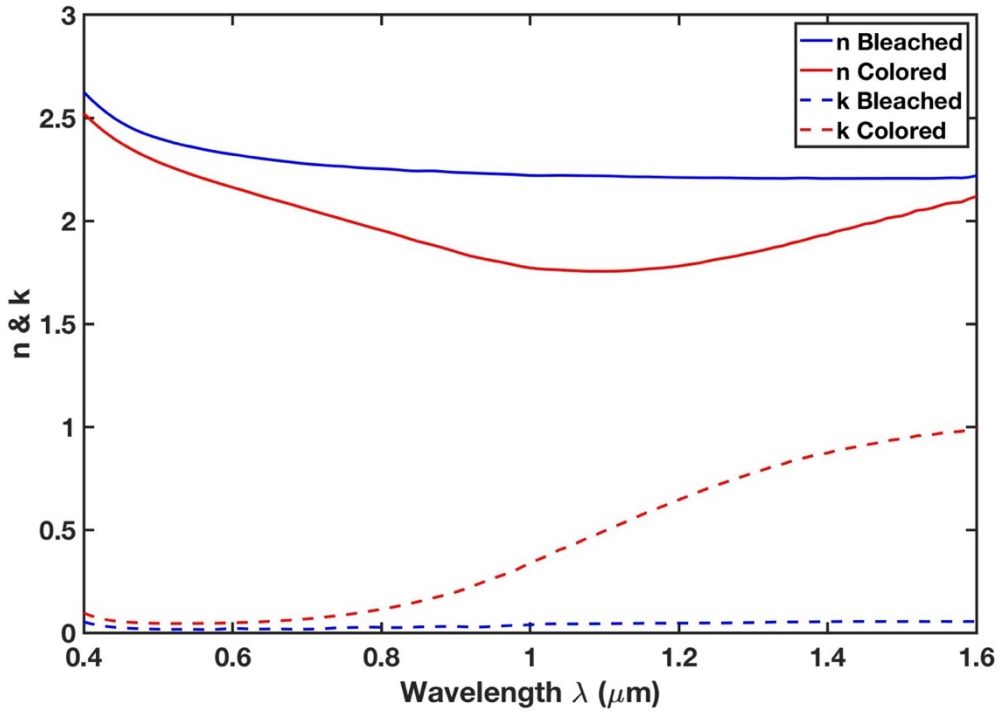

Figure 2.4: Tungsten trioxide (WO_3) refractive index (n) and absorptive index (k) over wavelengths 0.4 to 1.6 µm in both the colored and bleached states. Refractive index (n) solid line, absorptive index (k) solid line. The bleached state is in blue and the colored state is in red [17].

For tungsten trioxide we see that the bleached state has a slightly higher index of reflection meaning that it will reflect incrementally more. However, WO_3 in its bleached state also has a lower index of absorption which is almost zero which would indicate that as light passes through, it hardly absorbs anything allowing the rest of pass-through untouched. This would make sense since it is quite transparent in its bleached state and is the reason it has been looked at for smart window applications. In the colored state it has a lower reflective index but a significantly higher absorptive index at higher wavelengths.

2.3 Reflection and Transmission Theory of Single Interface

With the optical properties, n and k found, it is important to now use these defined terms, reflection, absorption, and transmission between the two surfaces or through a surface so that structure's optical reflection absorption can be found. To find this we first have to find reflectivity which is broken into a real and imaginary component. These are often turned parallel for real and perpendicular for imaginary referring to the axis's of the real and imaginary plane cross. To calculate reflectivity it is also broken into a real and imaginary component. Fortunately, it can be summarized in the case of a normal incidence, the real and imaginary parts. So that the real and imaginary are the same equation 2.3.1 [21].

$$\rho_{\perp} = \rho_{\parallel} = \frac{(n_1 - n_2)^2 + k_2^2}{(n_1 + n_2)^2 + k_2^2} \tag{2.3.1}$$

In the equation 2.3.1 the subscripts represent material one and material two optical properties. The parallel and perpendicular components of reflectivity can be added together to get total reflectivity by simply using equation 2.3.2 [21].

$$\rho_{12} = \frac{1}{2}(\rho_{\perp} + \rho_{\parallel}) \tag{2.3.2}$$

This equation can then be used to show the reflection of the single material and expanded upon to account for multiple materials.

2.4 Theoretical Model for Multilayer Thin Film Structures

The procedures needed to calculate spectral radiative properties in indirect method are used here and are based upon Wang. et al [4]. The more commonly used indirect method calculates the hemispherical reflectance and uses this to find the spectral directional emissivity.

The energy conservation which states that $\alpha'_{\omega} + R'_{\omega} + T'_{\omega} = 1$. Here it is quite clear to see that if the material is opaque there will be no transmissions through the material and as a consequence $T'_{\omega} = 0$ and the energy balance becomes much simpler $\alpha'_{\omega} = 1 - R'_{\omega}$. This can be seen by using the generalized Kirchoff law. We know that spectral directional emissivity and spectral directional absorptivity are equivalent $\alpha'_{\omega} = \varepsilon'_{\omega}$.

The Fabry–Pérot resonance cavity is used as an example, which is of particular interest since its architecture is being considered for the study's purpose. The emittance of a Fabry –Perot cavity can be calculated by summing the emissivity of the black body intensity for each of the layers.

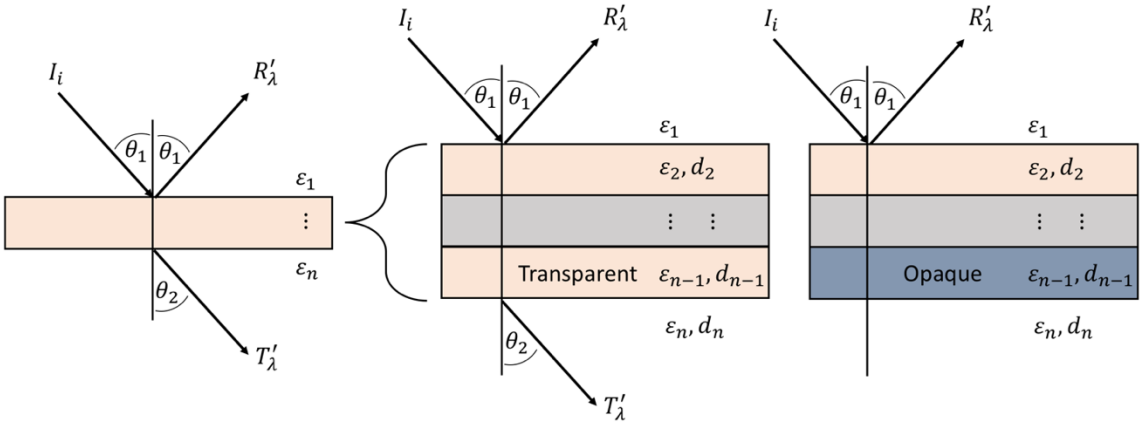

Figure 2.5: Shown are multilayered thin films. Far left is a simplified illustration showing spectral directional intensity interaction with the surface. All are showing transmitted, reflected, absorbed components of the incidence beam. Looking closer this is a stack of multiple thin layers. In the middle we have a semitransparent multilayered structure, and on the far right we have a multilayered structure with an opaque base.

The indirect method was utilized in our MATLAB based model. The indirect method only involves calculating the reflectance and transmittance of the structure in question. Looking at an electromagnetic wave that is incident on a multilayered structure single angle θ. Assuming each layer is homogeneous and isotropic, we can then model a TE wave at ω and being in the Jth layer of the structure.

$$E_j = E_{yj}\hat{y} = E_j(z)e^{i(\beta x - \omega t)}\hat{y} \tag{2.4.2}$$

Maxwell's equation can be used to find the magnetic field as follows:

$$H = \frac{1}{i\omega\mu\mu_o}\nabla \times E = \frac{1}{i\omega\mu\mu_o}\left(-\frac{dE_y}{dz}\hat{x} + \frac{dE_y}{zx}\hat{z}\right) \tag{2.4.3}$$

The pointing vector can be calculated after the magnetic and electric fields have been found. The component of the pointing vector in the z direction is as follows:

$$S_{1z} = \frac{\gamma_1}{2\omega\mu_0}(A_1A_1^* - B_1B_2^*) \tag{2.4.4}$$

And

$$S_{jz} = \frac{1}{2} Re\left[\frac{\gamma_j^*}{\omega \mu_0 \mu_j^*}(\psi_1 - \psi_2 - \psi_3)\right] \tag{2.4.5}$$

Here the ψ were defined as follows. $\psi_1 = \left|A_j\right|^2 e^{2\,Re(i\gamma_j)(z-z_{j-1})}, \psi_2 = \left|B_j\right|^2 e^{2\,Re(i\gamma_j)(z-z_{j-1})}$, and $\psi_3 = 2i\ Im\left[A_j B_j^* e^{2\,Im(i\gamma_j)(z-z_{j-1})}\right]$. Then after applying all of the boundary conditions the equation can greatly be simplified to the matrix form as follows.

$$\begin{pmatrix} A_j \\ B_j \end{pmatrix} = P_j D_j^{-1} D_{j+1} \begin{pmatrix} A_{j+1} \\ B_{j+1} \end{pmatrix} \tag{2.4.6}$$

The P_j is defined in the following way and is the propagation matrix.

$$P_j = \begin{pmatrix} 1 & 0 \\ 0 & 1 \end{pmatrix} \text{ when j=1} \tag{2.4.7}$$

And

$$P_j = \begin{pmatrix} e^{-i\gamma_j d_j} & 0 \\ 0 & e^{i\gamma_j d_j} \end{pmatrix} \text{ when j=2,3,…} \tag{2.4.8}$$

The D_j is defined in the following manner and is the dynamic matrix.

$$D_j = \begin{pmatrix} 1 & 1 \\ \gamma_j/\mu_j & -\gamma_j/\mu_j \end{pmatrix} \text{ when j=1,2,3, …} \tag{2.4.9}$$

It then can be shown that:

$$\begin{pmatrix} A_1 \\ B_1 \end{pmatrix} = M \begin{pmatrix} A_N \\ B_N \end{pmatrix} \tag{2.4.10}$$

Then the M must be the following:

$$M = \prod_{l-1}^{N-1} P_j D_j^{-1} D_{j+1} \tag{2.4.11}$$

Then we can find the transmissive and reflective coefficient.

$$t = \frac{A_N}{A_1} = \frac{1}{M_{11}} \tag{2.4.12,a}$$

$$r = \frac{B_1}{A_1} = \frac{M_{21}}{M_{11}} \tag{2.4.12,b}$$

The spectral directional-hemispherical reflectance then is defined as the following:

$$R'_\omega = rr^* = \left|\frac{M_{21}}{M_{11}}\right|^2 \tag{2.4.13}$$

And the spectral directional-hemispherical transmittance is:

$$T'_\omega = \frac{Re(\gamma_N/\mu_N)}{Re(\gamma_N/\mu_N)}\, tt^* = \frac{Re(\gamma_N/\mu_N)}{Re(\gamma_N/\mu_N)}\left|\frac{1}{M_{11}}\right|^2 \tag{2.4.14}$$

And finally, we can get the following

$$\alpha'_\omega = 1 - T'_\omega - R'_\omega \tag{2.4.18}$$

CHAPTER 3

OPAQUE STRUCTURES

3.1 Solar Spectrum

In this chapter a step-by-step process is used involving several structures of growing complexity. Starting from the simplest possible structure, a layer of tungsten trioxide, WO_3 at different thicknesses deposited on a layer of aluminum, these structures are explored. For the opaque surface such as aluminum the transmittance will be zero and as such is left off of the graphs completely. Next a bi-layered structure is explored, followed by a simple tri-layered architecture. The approaches explored in this chapter include the tri-layer structure construction that has a layer of tungsten trioxide on top of a thin layer of silica, on top of an opaque aluminum surface. These simple structures are explored, step by step through the design process. In this way one will be able to see how each layer changes the properties of the overall structure.

Before diving into each structure, it is important to remember that in order to propel any structures through space a radiation source will be needed. Naturally the sun provides a radiation source. It is important to understand that resources do not have consistent radiation intensity at all wavelengths of light. Due to this, the vast majority, roughly 80% of the solar energy falls between 0.4 nm and 1.6 nm and for the remainder of the analysis it is seen that this range is used. The rationale of using such a range is twofold. First with 80% being concentrated in a small range this is what this space device should be tuned to, and secondly most material property data obtained was over this range thus limiting the quality of the model outside of this range.

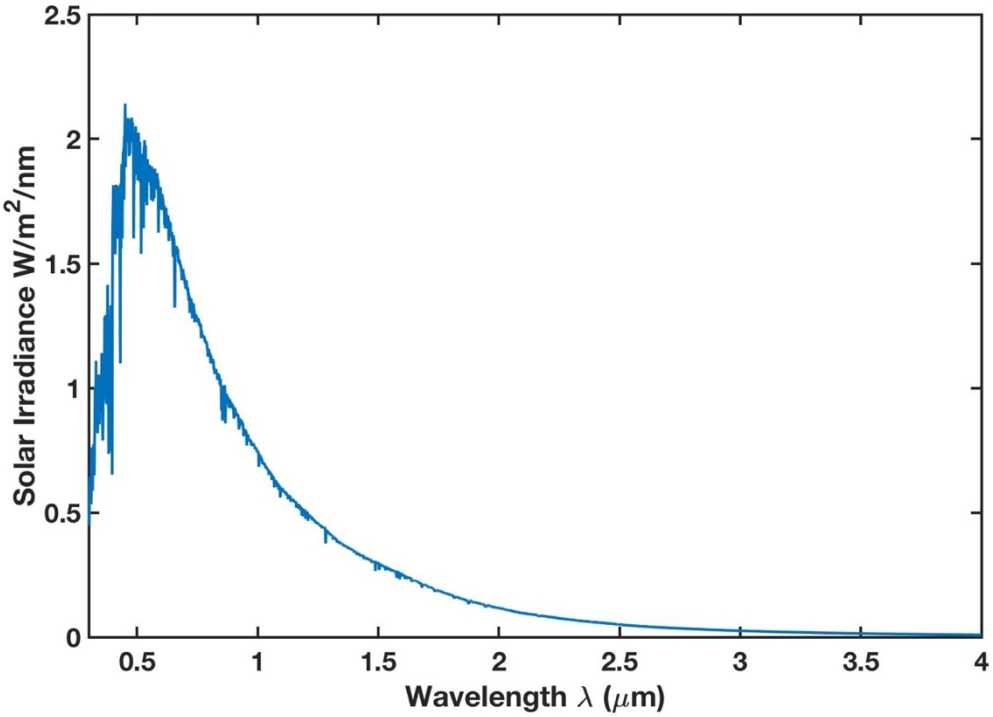

Figure 3.1: Extraterrestrial Solar Spectrum, over the range from 2.8 μm to 4 μm at one AU. Solar irradiation is seen to be strongest in the visible range 0.38 to 0.74 μm and steeply dropping off thereafter. The units used on the y-axis W/m^2/nm are customary to show the solar spectrum. However, they can be simplified to simply be W/m^3 a heat flux.

Solar spectral radiation I_λ plays a key role in the calculating of the total spectral reflection and for that matter transmittance. Fig. 3.1 is the solar spectrum at one AU the distance from the sun to the earth. Many space applications that may utilize solar sailing and radiation pressure modulation for steering will need to take this into account when calculating attitude maneuvers in deep space. For example, solar sailing is one of the most promising possibilities to leave the solar system. The distance of which is at 122 AU and will have a much smaller magnitude and may have a different profile from attenuation through the solar system.

3.2 Tungsten Trioxide (WO3) Deposited on Aluminum (Al)

The first structure that is explored is a simple single layer opaque structure, a layer of tungsten trioxide, WO_3 on an aluminum, Al wafer. This structure was meant to explore the properties of one of the simplest structures to be able to see the spectral changes between the bleached and opaque states. The simple structural diagrams is shown in Figure 3.2, showing a variable layer of tungsten trioxide (WO_3) on a semi incident layer aluminum wafer.

Figure 3.2: Simple schematic of tungsten trioxide, WO_3 which varies in thickness from 40 nm to 200 nm. This is deposited on a 200 nm thick aluminum, Al wafer. Aluminum at this thickness is opaque so that transmittance will be zero.

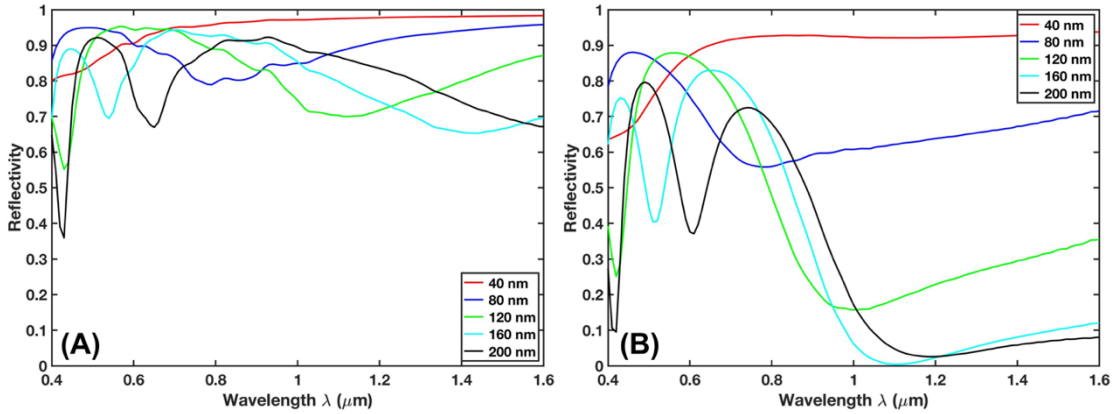

Figure 3.3: Spectral Reflectance of WO_3 on Al. A layer of tungsten trioxide, WO_3 is increased in thickness from 40 nm to 200 nm and is deposited on a 200 nm thick aluminum wafer. Reflectance shown by solid line. (**A**) shows bleached tungsten trioxide WO_3. (**B**) shows colored tungsten trioxide WO_3.

Observing Fig. 3.3 it can be observed that there is a significant change between the colored and the bleached states. In all thicknesses there is less reflection when tungsten trioxide is in its bleached Figure 3.3(B) when compared to the current Figure 3.3(A). As the thickness of the tungsten layer increases there is a decrease in the reflectivity of the surface. However, the change in reflectivity is greater than in the bleached state.

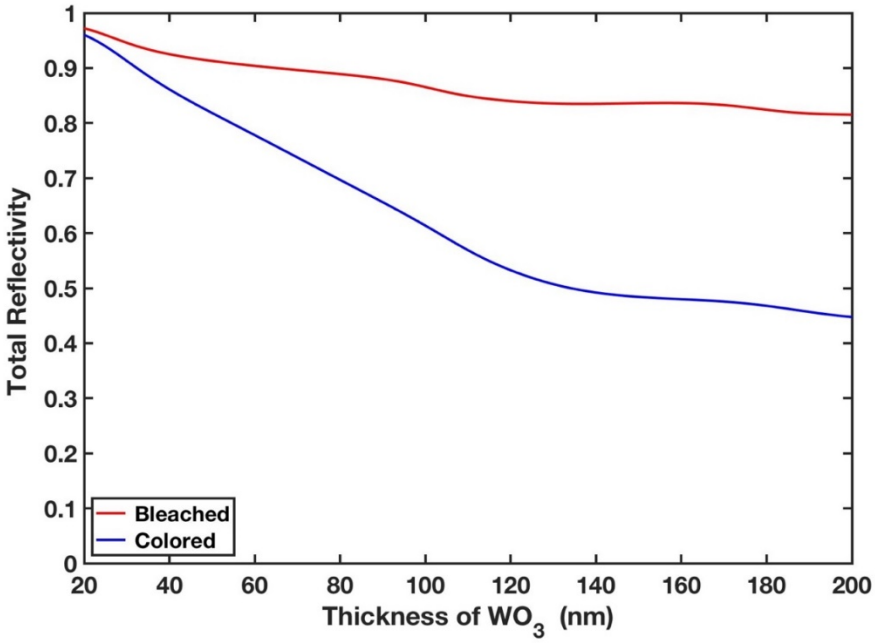

Figure 3.4: A layer of tungsten trioxide, WO_3 is increased in thickness from 20 nm to 200 nm and is deposited on a 200 nm thick aluminum wafer. On the horizontal axis the total reflectance is shown by solid lines, and the total transmissions is shown by dashed lines. The Red line represents the bleached state and the Blue line represents the colored state.

In order to calculate the total reflectivity over the spectrum an equation can be utilized as follows.

$$\rho = \frac{\int_{0.4\mu m}^{1.6\mu m} \rho_\lambda \, I_\lambda \, d\lambda}{\int_{0.4\mu m}^{1.6\mu m} I_\lambda \, d\lambda} \tag{3.2.1}$$

Integration in equation 3.2.1 ρ represents the total reflectivity. This is the spectral reflectivity (ρ_λ) multiplied by the spectral intensity mentioned earlier and is why the solar spectrum is so important. The model we used we utilized this solar spectrum as I_λ to give it practical results. Integrating over the solar spectrum from 0.4 to 1.6 μm and dividing by the actual solar intensities integrated on its own which would be the total radiation of the sun over the spectrum. Thus, the result is a spectral reflectivity between zero and one, one representing perfect reflectivity, and zero representing here perfect absorption.

It can be easily observed from this figure that the layer of tungsten trioxide, WO_3 deposited on an aluminum wafer increases in thickness causing the change between colored and bleached states increasing but then starting to level off around 150 nm.

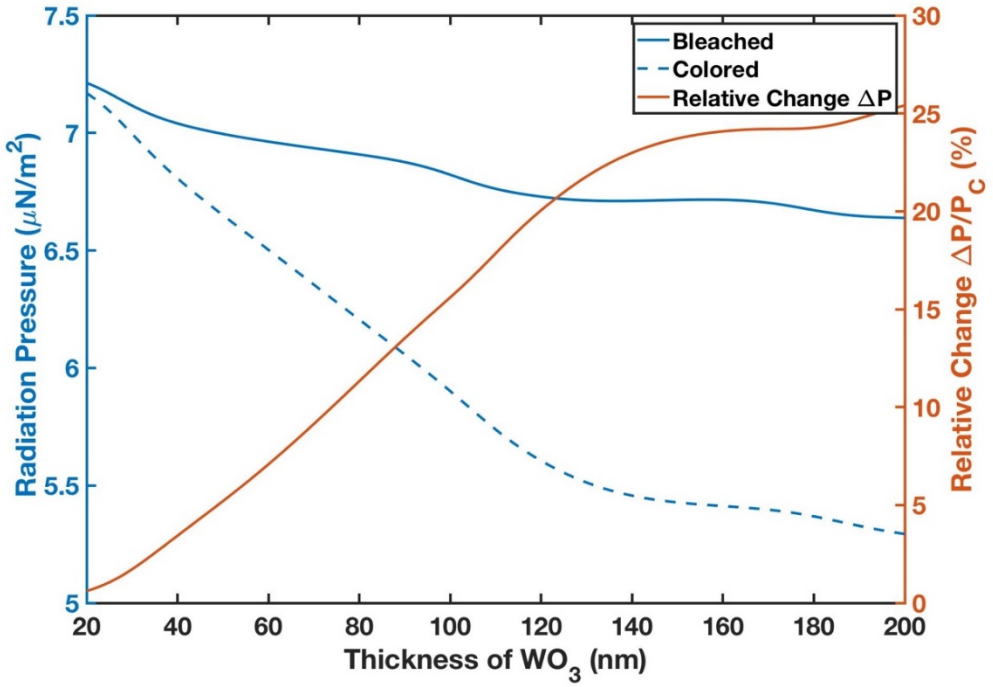

Figure 3.5: A layer of tungsten trioxide, WO_3 is increased in thickness from 20 nm to 200 nm and is deposited on a 200 nm thick aluminum wafer. Radiation pressure as shown on the left vertical axis in blue. The Blue dashed (---) line represents radiation pressure in the colored state. Blue solid (−) line represents the radiation pressure bleached state. The right vertical axis in red is the percent change between colored and bleached structures. The Red line represents the percent change in radiation pressure between the two colored and bleached states.

In this figure the percentage change in radiation was calculated using the following equation. In equation 3.2.2 P_b is radiation pressure of bleached WO_3 structure, and P_c is radiation pressure of colored WO_3 structure.

$$\%\Delta P = \frac{|P_b - P_c|}{P_b} 100\% \qquad (3.2.2)$$

In Fig. 3.5 it is easily observed that radiation pressure is less in the colored state than in the bleached state. It is also observed that as the layer of the tungsten trioxide increases so does the difference between the two. This can be understood better by observing the optical pressure creating equation 3.2.3.

$$P = \frac{1}{C}\int_{0.4\mu m}^{1.6\mu m} I_\lambda (2R_\lambda + A_\lambda)\, d\lambda \qquad (3.2.3)$$

Including in equation 3.2.3 C is the speed of light, $I_{\lambda i}$is the intensity of the solar spectrum, R_λ is the spectral radiation, and A_λ is the spectral absorption. Transmission does not affect radiation pressure because it just passes through the material.

Working with an opaque material the transmission is zero. Radiation plus absorption will equal one. Equation 3.3 shows us that reflection is twice as important as absorption in increasing radiation pressure. The bleached state shows more radiation pressure and is not in line with this idea to have lower radiation pressure since it also shows a higher level of reflection. The opposite can be said for the color state which does not have a lower level of reflection but will have a lower optical pressure.

3.3 Tungsten Trioxide (WO3) on Silicon (Si) on Aluminum (Al)

A three-layered opaque structure featuring a tungsten trioxide top layer, a silicon middle layer and an aluminum base. This structure proposed here is hoped to utilize a Fábry Perot cavity which is when the WO_3 is in the colored state and is hoped to increase absorption in the physical and infrared ranges. Fabry Perot resonance occurs when two mirrors are utilized and light bounces between the two, in this case tungsten trioxide would be the top layer and aluminum would be the bottom mirror layer in the colored state.

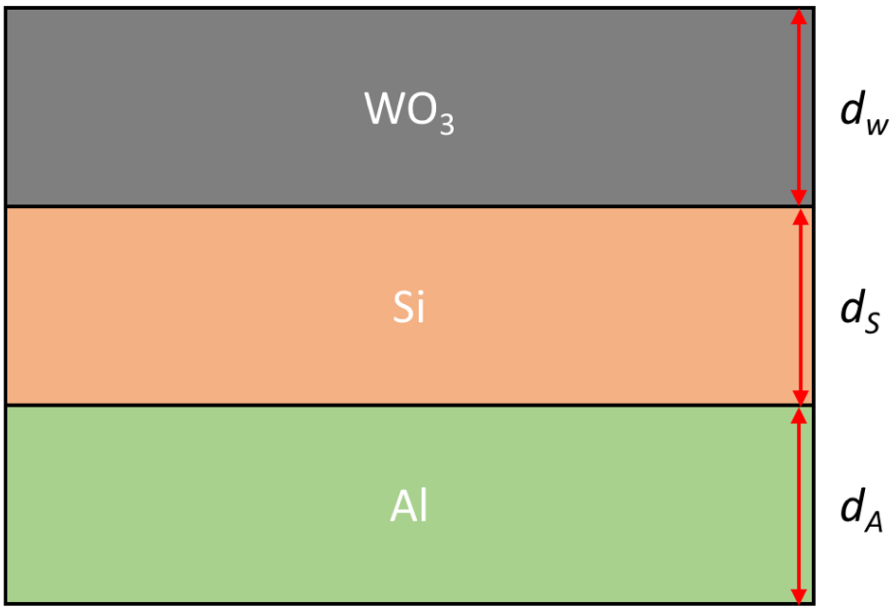

Figure 3.6: Simple schematic of tungsten trioxide WO_3 which varies in thickness from 20 nm to 200 nm, the second layer is 50 nm of silicone Si, and the base is 200 nm of aluminum Al wafer. Aluminum at this thickness is opaque so that transmittance will be zero.

Tungsten trioxide thickness d_w is varied from 20 nm to 200 nm, silicon is held constant at 50 nm and aluminum is relatively thick at 200 nm. Later silicon thickness d_s is varied from 20 nm to 200 nm, tungsten trioxide is held constant at 200 nm and aluminum thickness d_A is held constant at 200 nm.

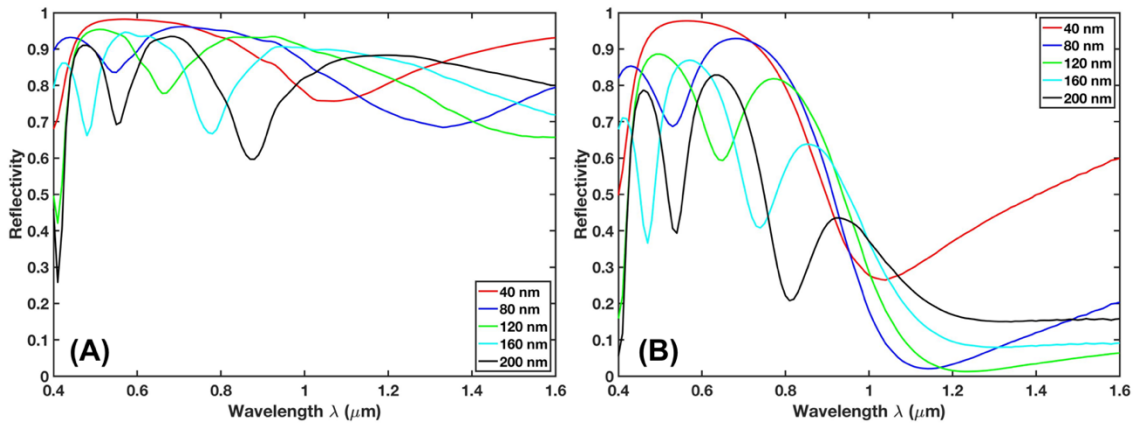

Figure 3.7: A layer of tungsten trioxide, WO_3 is increased in thickness from 40 nm to 200 nm with a 50 nm Si layer in the middle and a 200 nm aluminum surface on the bottom. Reflectance shown by solid lines. (**A**) shows bleached tungsten trioxide WO_3. (**B**) shows colored tungsten trioxide WO_3.

In Fig. 3.7 it is seen that in the bleached state there is more reflection especially at lower wavelengths. In the colored state observed, that reflection is only slightly decreased at low wave lengths and is very decreased at high wavelengths. This steep drop off is often seen with the use of the Fábry Perot cavity increasing absorption. However above one micrometer the solar spectrum drops off in intensity so that the fact of having a higher absorption and as a result a lower reflection is not as great as it would have been if it would have dropped off any lower in wavelength.

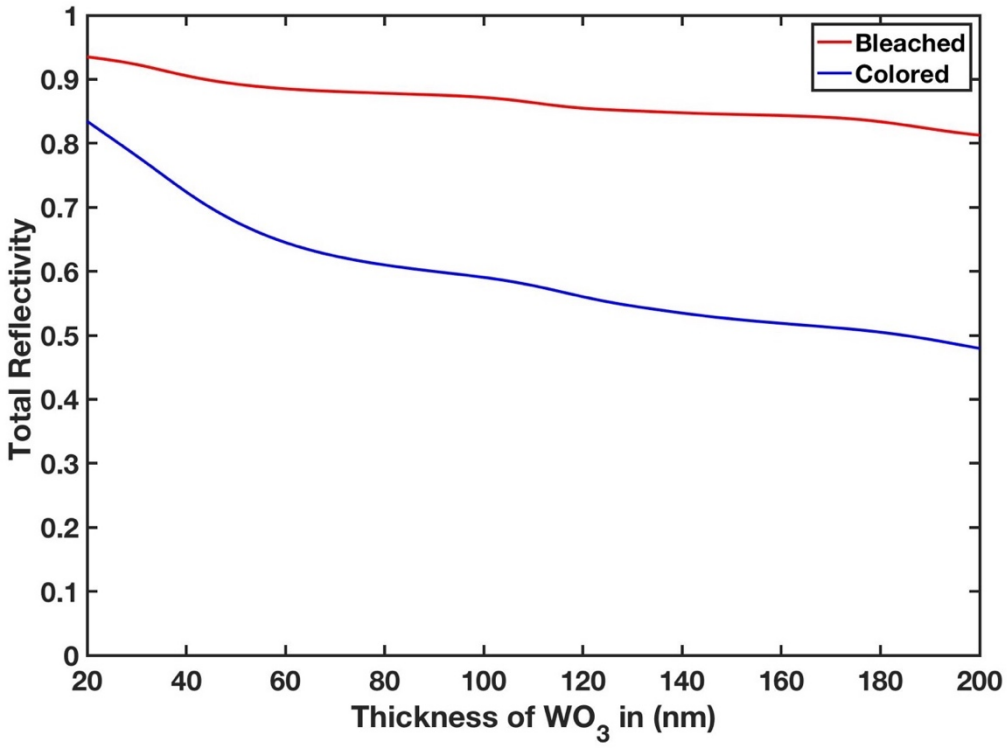

Figure 3.8: A layer of tungsten trioxide, WO_3 is increased in thickness from 20 nm to 200 nm with a 50 nm Si layer in the middle and a 200 nm aluminum surface on the bottom. The horizontal axis is thickness, the vertical axis is total reflection. The solid blue line is the total reflection when tungsten trioxide is in its colored state. The solid red line is total reflection when tungsten trioxide is in its bleached state.

Here we can see the difference in reflection between the two states; colored and bleached increase as the thickness increases. However, after around 150 nm thick WO_3, the lines continue to decrease but are running almost in parallel. This as a result changes between the total reflection and becomes almost constant as the thickness increases.

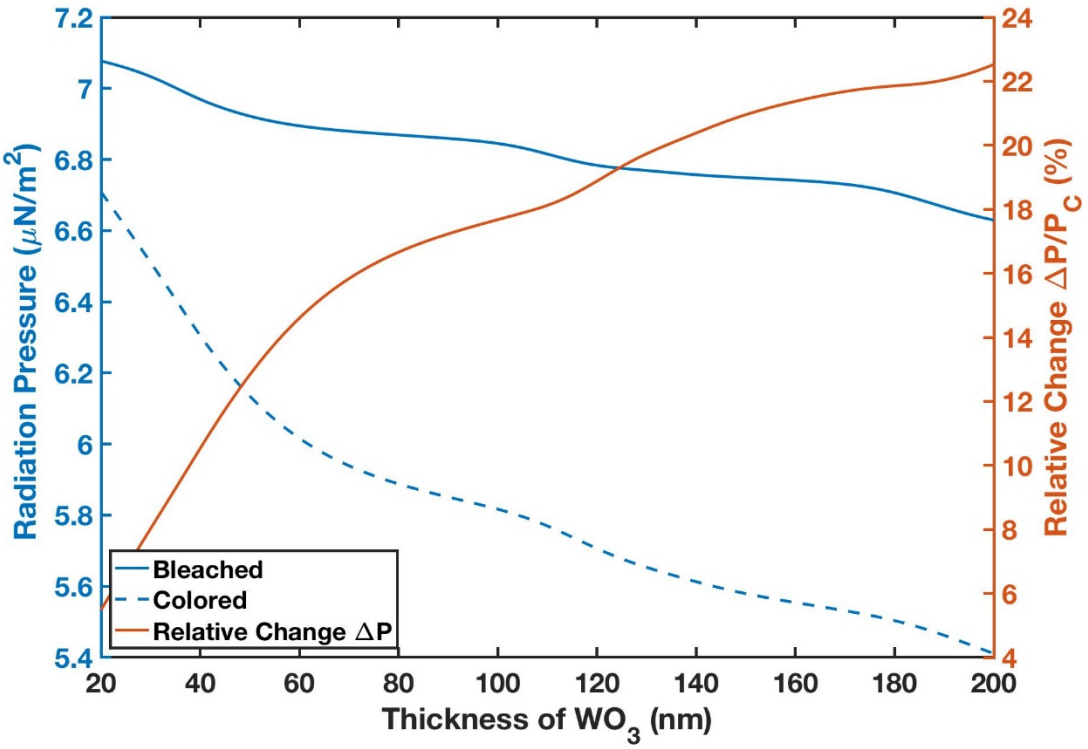

Figure 3.9: A layer of tungsten trioxide, WO_3 is increased in thickness from 20 nm to 200 nm with a 50 nm Si layer in the middle and a 200 nm aluminum surface on the bottom. Radiation pressure is shown on the left vertical axis in blue. The Blue dashed (---) line represents radiation pressure in the colored state. The Blue solid (−) line represents the radiation pressure in bleached state. The right vertical axis in red is the percent change between colored and bleached structures. The Red line represents the percent change in radiation pressure between the two colored and bleached state.

Observe from Fig. 3.9 that the bleached state has higher radiation pressure, and the colored state has a lower radiation pressure. As was mentioned earlier this can be explained by equation 3.3 that shows that reflection is twice as important as absorption in its effect on radiation pressure. Thus, as we did before it could be predicted that because each state has higher total reflection it will also have higher radiation pressure. As the thickness of the tungsten trioxide layer increases so does the percent change in radiation pressure which was calculated by equation 3.4. The trend of the percent change curve would indicate that

the optimal tungsten trioxide thickness would be around 200 nm or slightly above to maximize the change in optical force.

With this knowledge of maximum radiation pressure changing at a thickness of 200 nm of tungsten trioxide, this was set to be the constant and the silicone was varied from 20 to 200 nanometers in order to observe the change in this layer. The total reflectivity versus thickness of silicone, Si is graphed in Fig. 3.10.

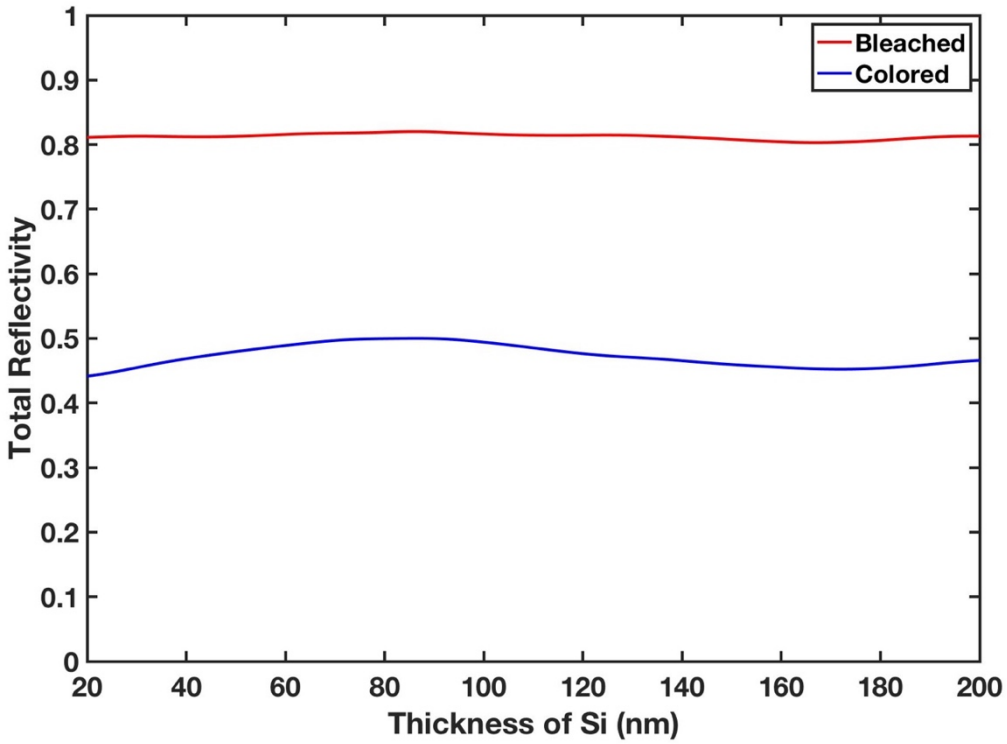

Figure 3.10: The top layer is a 200 nm thick layer of tungsten trioxide, WO_3, the middle layer is silicon, Si varying from 20 nm to 200 nm in thickness and then the 200 nm aluminum surface on the bottom. The horizontal axis is thickness. The vertical axis is total reflection. The solid blue line is the total reflection when tungsten trioxide is in its colored state. The solid red line is total reflection when tungsten trioxide is in its bleached state.

From the Figure 3.10 it appears that reflectivity in the bleached state is relatively constant regardless of the thickness of silicone. However, there is some variation in the reflectivity of this structure with thickness in its colored state.

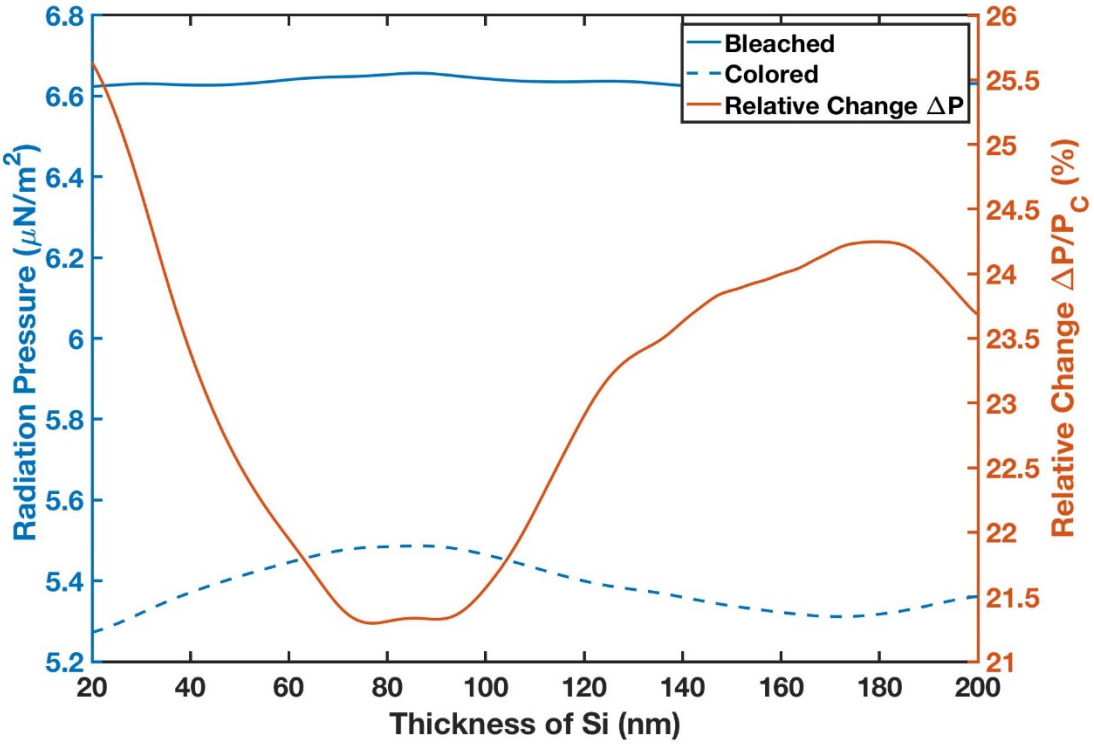

Figure 3.11: The top layer is a 125 nm thick layer of tungsten trioxide, WO_3. the middle layer is silicon, Si varying from 20 nm to 200 nm in thickness and then the 200 nm aluminum surface on the bottom. Radiation pressure is shown on the left vertical axis in blue. The Blue dashed (---) line represents radiation pressure in the colored state. The Blue solid (−) line represents the radiation pressure in the bleached state. The right vertical axis in red is the percent change between colored and bleached structures. The Red line represents the percent change in radiation pressure between the two colored and bleached states.

In order to observe the affect this has on radiation pressure the same variation in silicone thickness was graphed as well as the relative change in radiation pressure. From Fig. 3.11 it can be seen that there are two peaks. The first is at 20 nm of silicone which

allows over a 25.5% relative change. The other is much thicker at 180 nm silicone and produces a 24% relative change.

The observation that varying both tungsten trioxide as well as silicone both result in distinct peaks and valleys. This leads to the desire to have a contour plot varying both WO_3 and Si simultaneously to observe the interactions and show where the best results could be obtained. This led to the construction of Figure 3.3.7.

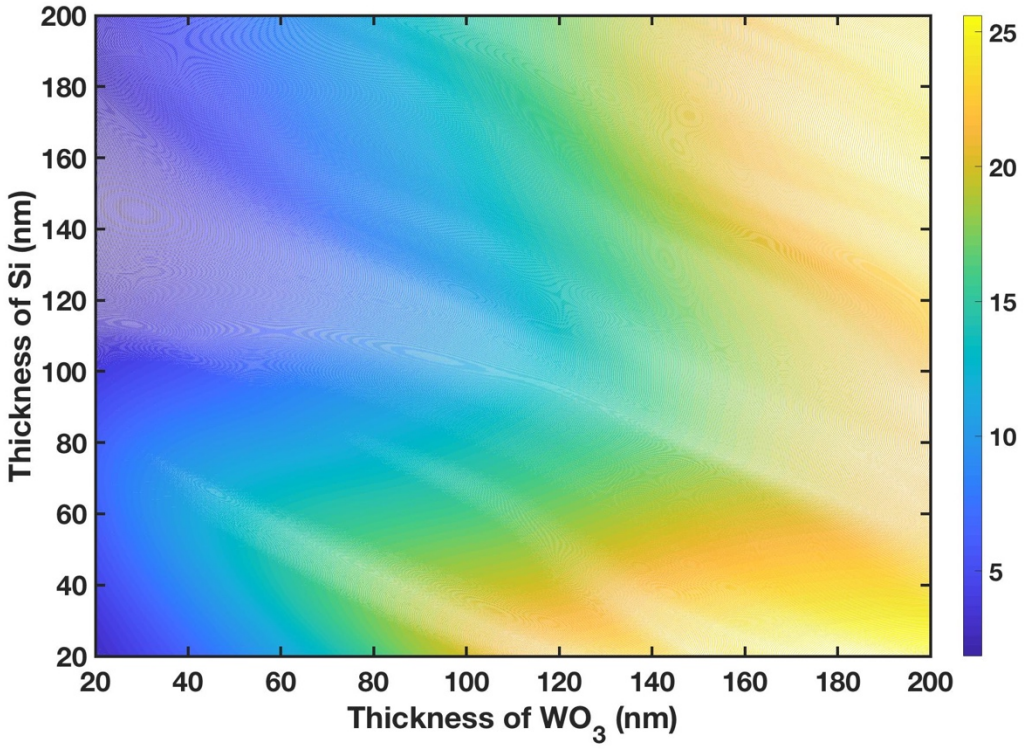

Figure 3.12: A top layer of tungsten trioxide, WO_3 varies from 20 nm to 200 nm, a middle layer of silicon, Si varies from 20 nm to 200 nm, and a 200 nm aluminum surface on the bottom. The contour plot is of WO_3 thickness, Si thickness, and percent relative change [%]. The Vertical axis is the thickness of the silicone, Si. The horizontal axis is the thickness of tungsten trioxide, WO_3. The color scheme is percent relative change [%].

It is observed from Fig. 3.12 that the best results are at relatively high tungsten trioxide thickness as can be observed from the wider colors on the right-hand side. Furthermore, it is also shown that there is a bi lobed distribution for silicone showing that

at a relatively small thickness of 20 nm it has its maximum value over 25 percent relative change in radiation pressure. It is also seen that at 180 nm thickness of silicone there is a similar magnitude of relative change in radiation pressure.

The two structures observed here, at first glance would yield the result that a 25% change occurs with the two layered structure seen in Figure 5. This would be preferable over a three-layered structure with a 23% change in radiation pressure. Upon further analysis of the three-layered structure it is found that by varying the silicone layer in addition to the tungsten trioxide layer, it is possible to increase the reflectivity to 25%. This observation can easily be seen in Figure 3.3.7 which varies both silicone and tungsten trioxide layers simultaneously. Observation shows that material interactions in varying thicknesses lead to an improved result creating opportunity for future research of these structures. This opens the door for further research in this area and makes tungsten trioxide a promising material for radiation pressure applications.

CHAPTER 4

SEMI-TRANSPARENT STRUCTURES

4.1 Single Layer of Tungsten Trioxide WO_3

In the last chapter the exploration of opaque surfaces was taken on. In this chapter we will explore surfaces capable of becoming semitransparent. A semitransparent structure offers the advantage of having a very low radiation pressure and with a phase change to a reflective surface could offer a high level of modulation between these radiation pressures. For this reason, the possibility of utilizing semitransparent structures is explored.

Much as in the previous chapter a step by step systematic approach is taken. Starting from a single layer of tungsten trioxide, WO_3, which is a less than realistic structure for practical use but a nice modeling tool to see the behavior of WO_3 on its own. This is followed by a layer of tungsten trioxide on a layer of silicone, which leads to the tri-layered structure which uses the Fábry Perot resonance cavity to increase reflectivity. This will utilize two layers of WO_3 sandwiched between layers of silicone. These structures are hoped to lead to a better understanding of the utilization of WO_3 radiation force applications and the potential of utilizing semitransparent structures.

The first structure explored is a simple single layer of WO_3. This would not be a practical architecture for any application however it is useful to observe reflection and transmission of this naked material.

Figure 4.1: A single layer of tungsten trioxide varying from 20 nm to 200 nm, in steps of 40 nm.

In Fig. 4.1 the simplest of structures illustrated a solo layer of concentrate outside and is modeled and is used to observe the reflection and transmission of WO_3.

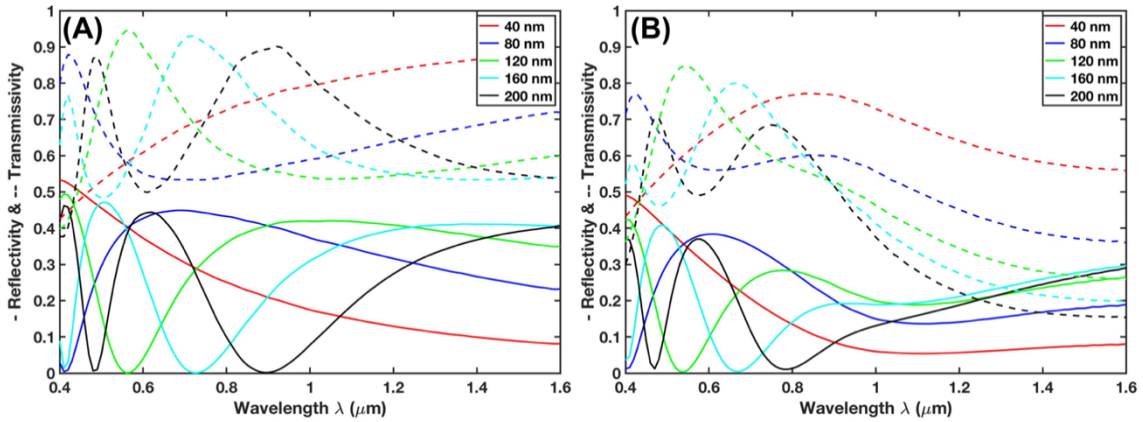

Figure 4.2: Single layer of tungsten trioxide, WO_3 varying in thickness from 40 nm to 200 nm. Reflectance is shown by solid lines, and transmission is shown by dashed lines. (**A**) shows bleached tungsten trioxide WO_3. (**B**) shows colored tungsten trioxide WO_3.

In Fig. 4.2, it is observed transmittance is actually significantly higher than reflection as a general trend in both the colored and bleached states. Furthermore, in Fig. 4.2(A) the bleached state activity seen has thickness increases. There is a high transmittance and low reflection peak at low wavelengths that progresses to higher wavelengths as thickness increases. Fig. 4.2(B) it is seen that both reflection and transmission are impeded as thickness increases compared to the bleached state. These high

absorption peaks that can be seen in both state's position will greatly affect the total reflection and transmittance.

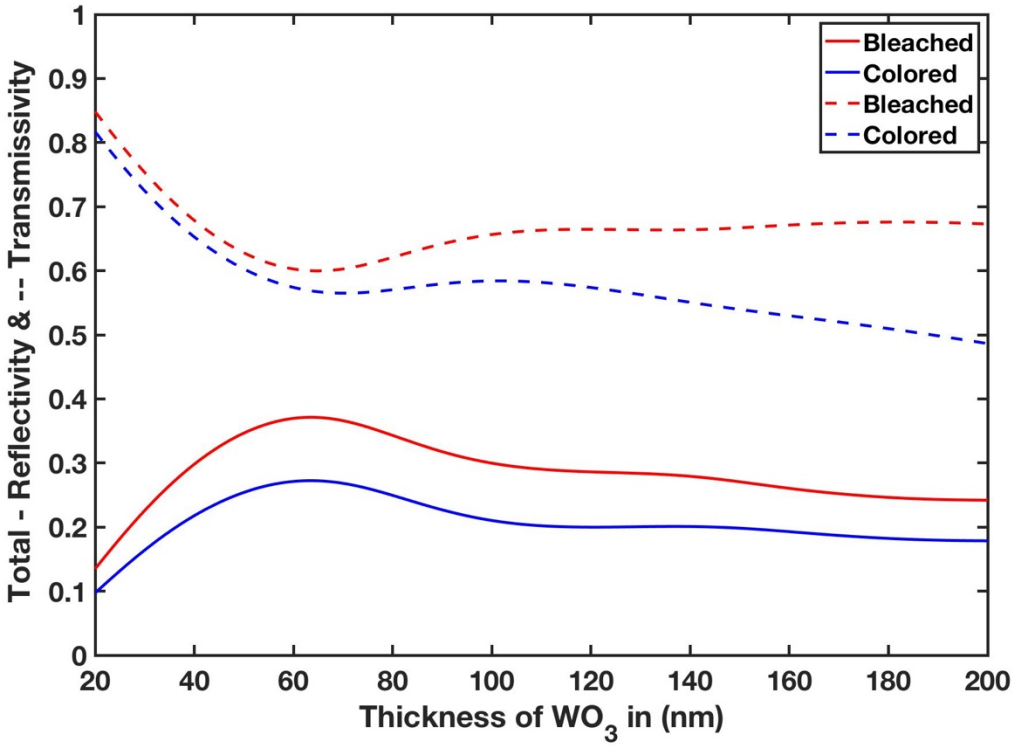

Figure 4.3: Single layer of tungsten trioxide, WO_3 is increased in thickness from 20 nm to 200 nm, on the horizontal axis. Total reflectance is shown by solid lines, and total transmission is shown by dashed lines. The Red line represents the bleached state. The Blue line represents the colored state.

From Fig. 4.3 it can be said that as the layer of tungsten trioxide, WO_3 increases in thickness the change between colored and bleached states increase, for both transmittance and reflectance. There is a peak in total reflectance at around 60 nm. However, there is a corresponding dip in total transmittance. This is seen across bleached and colored substances. There is a remarkably consistent difference between the reflected state of the colored and bleached states regardless of thickness. This data allows us to see that there might be an advantage to having a 60 nanometers thick tungsten layer. It also shows that

at higher thicknesses there is a slight increase in separation between the transmissions of the two states. As thickness increases there is a very slight decrease in transmittance and reflectance indicating that there will be an increasing absorption.

4.2 Tungsten Trioxide On Silicon

In line with a simple approach, the simplest realistic design was analyzed here. A layer of tungsten trioxide, WO_3 which is varied in thickness in the section to come, is deposited on a 200 nm thick silicon wafer. This silicon is semitransparent and thus the hope is that we should have a realistic structure that functions between transparent and reflective in order to maximize solar sailing capability.

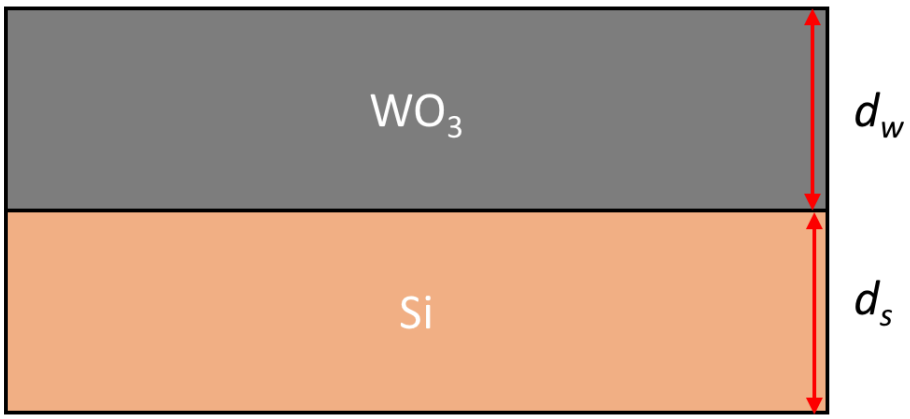

Figure 4.4: A layer of tungsten trioxide varies from 20 nm to 200 nm in steps of 20 nm on a 200 nm thick layer of silicon.

The structure is hoped to promote the transparent quality of WO_3 in its bleached state. It is bi layered with silicon, a natural semi-conductor, which is semitransparent over the solar spectrum.

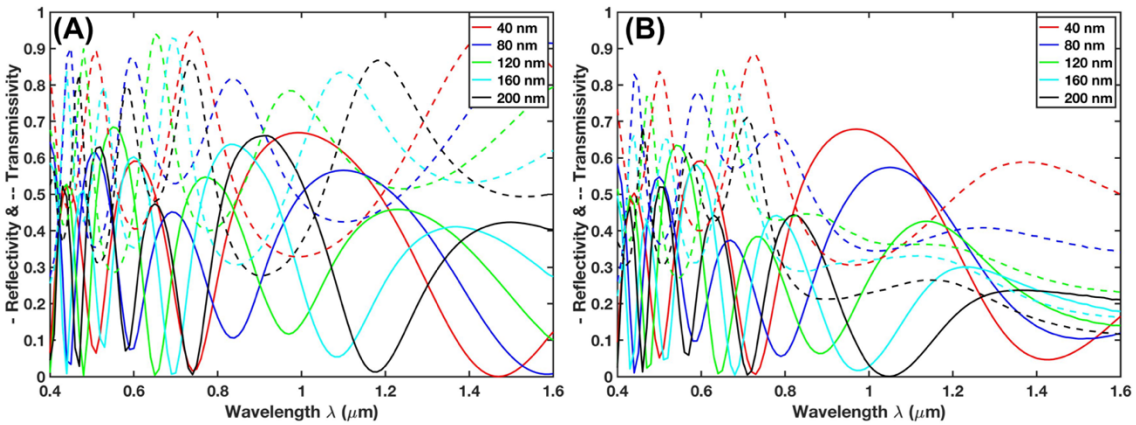

Figure 4.5: A layer of tungsten trioxide, WO_3 varying in thickness from 40 nm to 200 nm on a 200 nm thick silicon wafers. Reflectance shown by solid lines, and transmissions shown by dashed lines. (**A**) shows bleached tungsten trioxide WO_3. (**B**) shows colored tungsten trioxide WO_3.

A combination of silicon and tungsten each contribute their own absorption peaks which we see as waves in both the transmission and reflection. These peaks shift to higher wavelengths as thickness increases. As before there is an overarching trend as thickness increases transmittance and reflectance decrease. There is a noticeable difference between the transmittance between the colored sample (B) and the bleached sample (A). Reflection seems to be slightly less muted than transmission but it is still decreased.

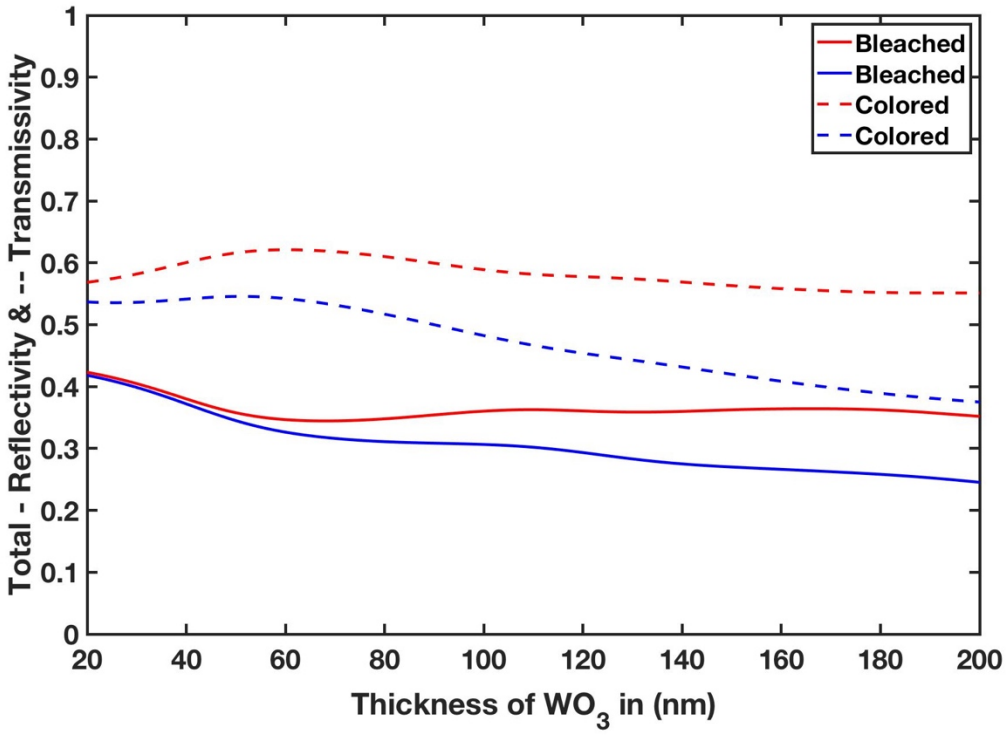

Figure 4.6: A layer of tungsten trioxide, WO_3 varying in thickness from 20 nm to 200 nm on a 200 nm thick silicon wafers. Total reflectance shown by solid lines, and total transmissions shown by dashed lines. The Red line represents the bleached state. The Blue line represents the colored state.

In Fig. 4.6 it is noted that total reflection is slightly higher than total transmittance. However, it is also noted that as thickness increases both total transmittance as well as total reflection diverge from each other between the bleached and colored state. This indicates that with this structure increased thickness will promote higher changes in radiation pressure.

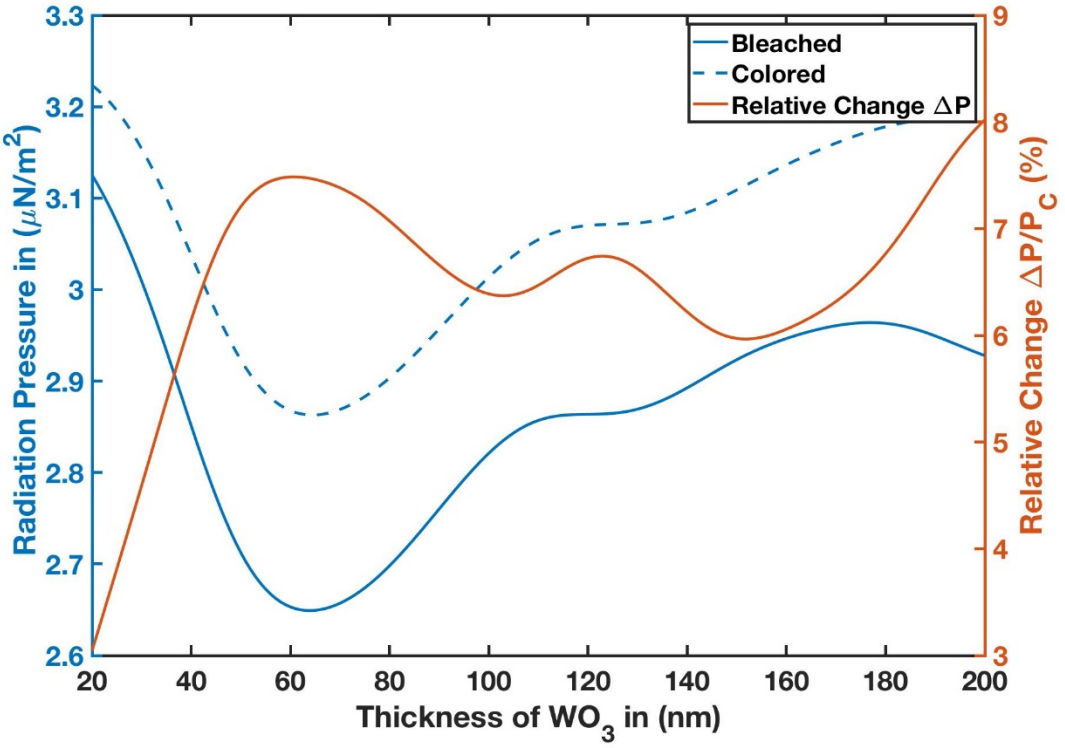

Figure 4.7: A layer of tungsten trioxide, WO_3 is increased in thickness from 20 nm to 200 nm and is deposited on a 200 nm thick silicon wafer. Radiation pressure is shown on the left vertical axis in blue. The Blue dashed (---) line represents radiation pressure in the colored state. The Blue solid (−) line represents the radiation pressure in the bleached state. The right vertical axis in red is the percent change between colored and bleached structures. The Red line represents the percent change in radiation pressure between the two colored and bleached states.

Observations from Fig. 4.7 yield that the rated pressure between the colored, a slightly higher reflectivity and the bleached, a slightly lower reflectivity, both follow the same general profile. As noted in the single layered structure there was a peak around 60 nm thickness tungsten and a note was made that this might be a useful thickness for an application. Here again we see a relative maximum percentage change in radiation pressure at around 60 nm. However, this is dwarfed in comparison to that seen at 200 nm WO_3. The trend in Fig. 4.7 would be that an even thicker layer of tungsten trioxide may provide even a better result than seen here. However, with the maximum percent change in optical

pressure of 8% this particular structure does not show much promise for an optical force modulation for space applications.

4.3 Tungsten Trioxide (WO_3) on Silicon(Si) on Tungsten Trioxide (WO_3)

The idea is to increase reflection and absorption using the three-layer structure of WO_3/Si/WO_3 to take advantage of the Fábry Perot resonance cavity in the colored state. It is hoped that the surface of this structure and its bleached state will still act semitransparent and therefore have a very low optical force.

Figure 4.8: A top layer of tungsten trioxide, WO_3 varies from 20 nm to 200 nm, a middle layer 50 nm thick silicon, and a bottom layer of WO_3 vary from 20 nm to 200 nm.

Tungsten trioxide is functioning as both the top and bottom here in a Fábry Perot cavity which traps light between the mirrors and increases absorption of light. This structure hopes to increase the optical force during its colored state when tungsten trioxide is more reflective and less transparent.

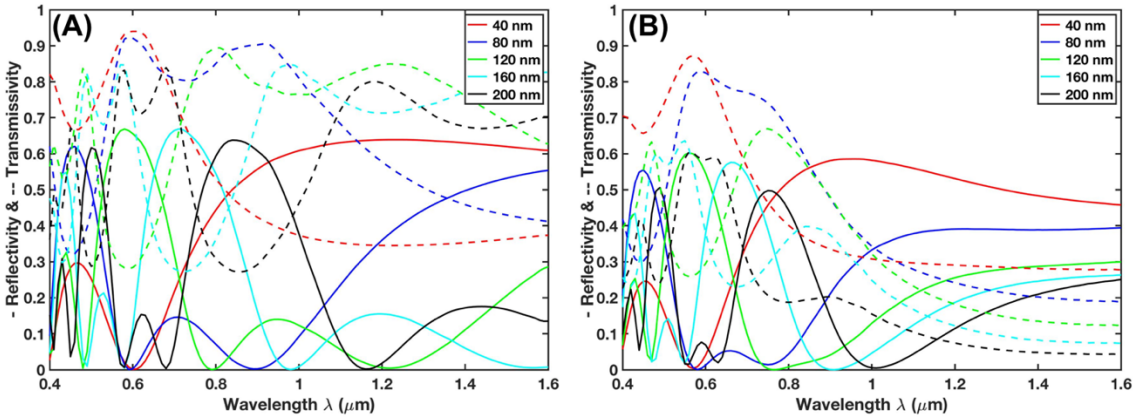

Figure 4.9: A top layer of tungsten trioxide, WO_3 varies from 40 nm to 200 nm, a middle layer 50 nm thick silicon, and a bottom layer of WO_3 varies from 40 nm to 200 nm. Reflectance is shown by solid lines, and transmittance is shown by dashed lines. (**A**) shows bleached tungsten trioxide WO_3. (**B**) shows colored tungsten trioxide WO_3.

In the bleached state we see a higher transmittance in the low wavelength range, between 0.4 - 0.6 micrometers. This disappears as tungsten trioxide increases in thickness. However, this could show promise in modulating radiation pressure. We do see a rise in reflection and a decrease in transmittance in the higher wavelengths. However, less of this solar spectrum is in these ranges thus it will affect total properties less. In the bleached state in Fig. 4.9(B) we see that there is a decreased in transmittance and much smaller decrease in reflectance at low wavelengths. At higher wavelength there is a dramatic decrease in transmittance and a decrease in reflection.

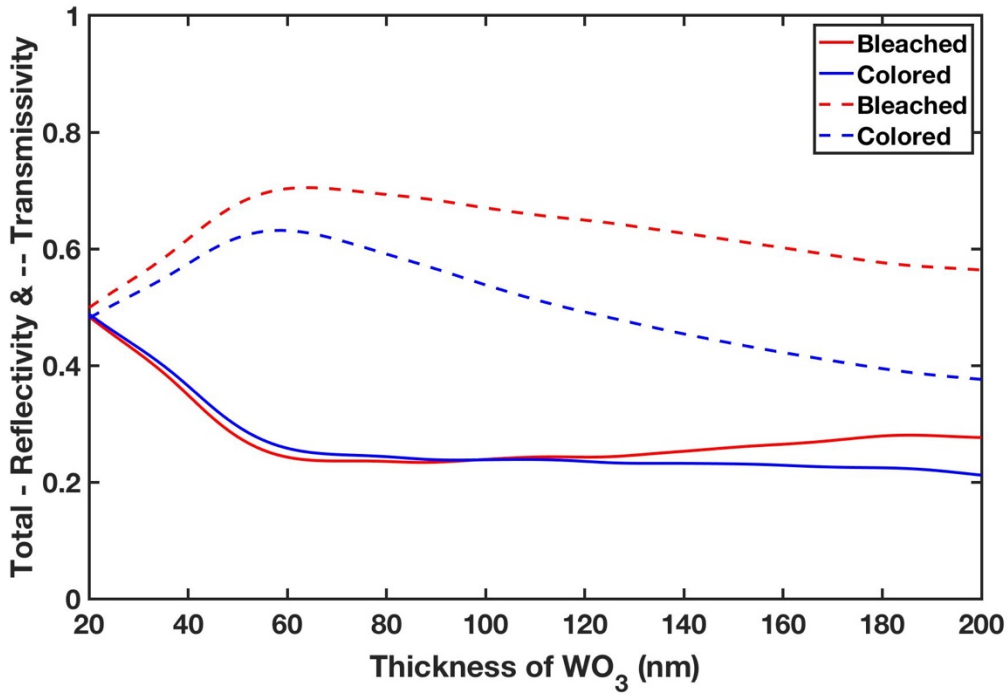

Figure 4.10: A top layer of tungsten trioxide, WO_3 varies from 20 nm to 200 nm, a middle layer of 50 nm thick silicon and a bottom layer of WO_3 varies from 20 nm to 200 nm. Total reflectance is shown by solid lines, and total transmission is shown by dashed lines. The Red line represents the bleached state. The Blue line represents the colored state.

The trend of having more transmittance and reflectance continues in Fig. 4.10 as well as having the bleached state have more transmittance. However, for reflection in Fig. 4.10 the colored and bleached states are almost on top of each other until they begin to separate at 120 nm thick WO_3 at which point they slowly diverge with the bleached state having more reflection. It is interesting to note that there is the greatest degree of difference in reflection and transmission at around 60 nm.

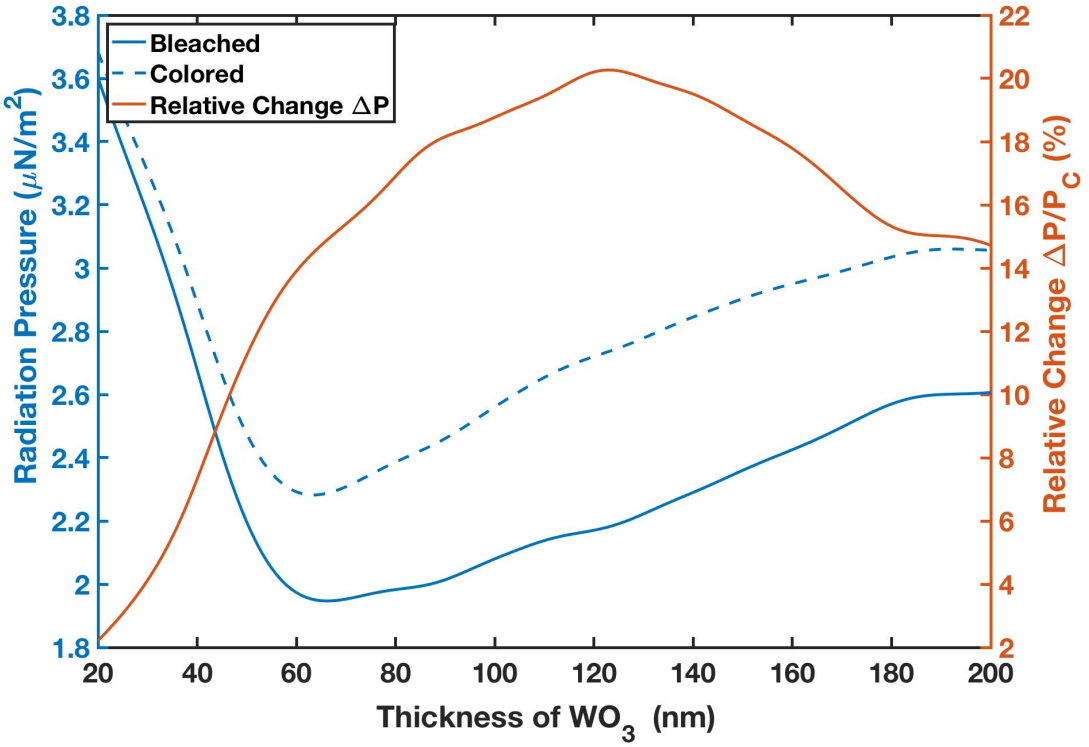

Figure 4.11: A top layer of tungsten trioxide, WO_3 varies from 20 nm to 200 nm, a middle layer of 50 nm thick silicon, and a bottom layer of WO_3 varies from 20 nm to 200 nm. Radiation pressure is shown on the left vertical axis in blue. The Blue dashed (---) line represents radiation pressure in the colored state. The Blue solid (−) line represents the radiation pressure in the bleached state. The right vertical axis in red is the percent change between colored and bleached structures. The Red line represents the percent change in radiation pressure between the two colored and bleached states.

We see that the trend of the radiation pressure in both colored and bleached states are very similar in profile shown in Fig. 4.11. The radiation pressure decreases for both states until approximately 65 nm and then WO_3 increases from thereafter. The percentage change in radiation pressure is seen to be maximum at approximately 120 nm. Looking back at Fig. 4.11 you will see that at around 110 nm the reflection lines between the colored and bleached state cross switching positions. Remembering back to equation 3.3 reflection is twice as important as absorption. In the current structure the colored state is the one with a higher optical pressure. To maintain this, we want the colored state to have the higher

reflection. In Fig. 4.11 we see that there is a transition to the bleached state having a higher reflectivity and thus leading to a decrease in the difference between the optical pressures. Figure 4.11 also shows us that this structure has a peak and has over a 20% change between the radiation pressure of the colored and bleached states.

As we observe with our opaque structures varying the center silicon has an impact on total reflectivity and here transmittivity as well. Thus, we set out to vary the silicone layer from 20 nm to 200 nm. From the Fig. 4.11 a peak in relative change of radiation pressure was seen with a tungsten trioxide layer of approximately 125 nm. This led to the decision to use 125 nanometer thick tungsten trioxide to be held constant in the next two Figs. 4.12 and 4.13.

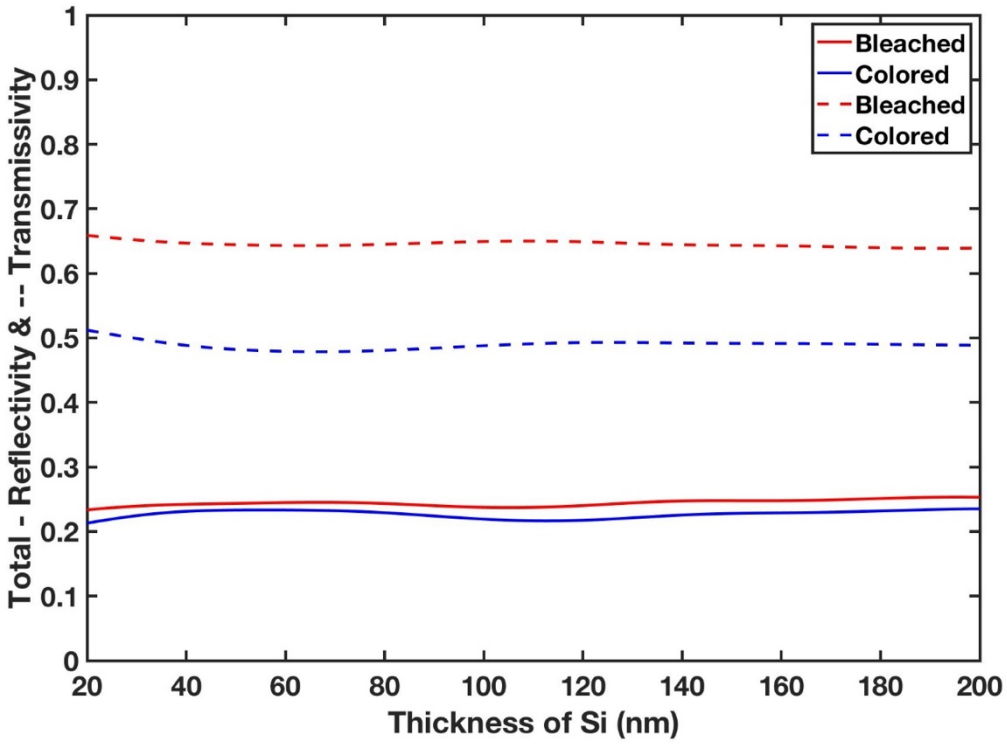

Figure 4.12: The top layer is a 125 nm thick layer of tungsten trioxide, WO_3 the middle layer is silicon, Si varying from 20 nm to 200 nm in thickness and then the 125 nm tungsten trioxide, WO_3 bottom layer. Total reflectance is shown by solid lines, and total transmission is shown by dashed lines. The Red line represents the bleached state. The Blue line represents the colored state.

It is seen from Fig. 4.12 that there is only slight variations in total reflectivity and transmittivity when varying silicone, Si from 20 nm to 200 nm. There is a slight increase in reflectivity and decrease in transmittivity as silicon gets thicker for both the colored and bleached states of tungsten trioxide. To see how this affects radiation pressure as well as changing radiation pressure Fig. 4.13 was created.

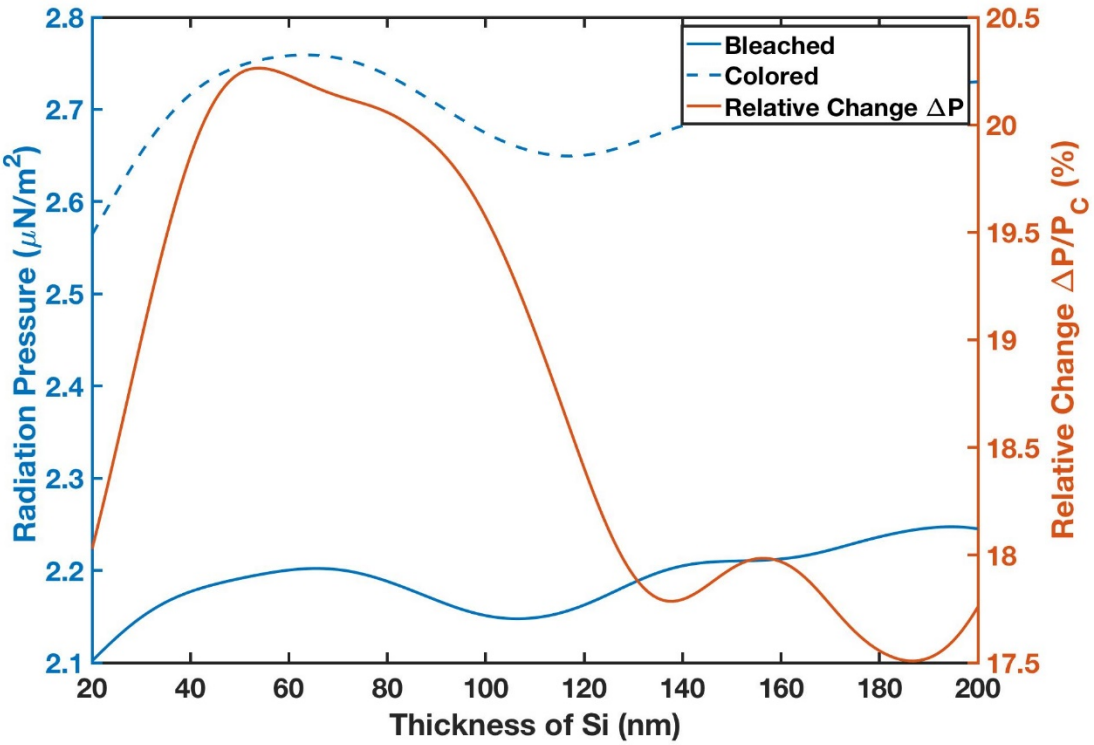

Figure 4.13: The top layer is a 125 nm thick layer of tungsten trioxide, WO_3, the middle layer is silicon, Si varying from 20 nm to 200 nm in thickness and then the 125 nm tungsten trioxide, WO_3 bottom layer. Radiation pressure is shown on the left vertical axis in blue. The Blue dashed (---) line represents radiation pressure in the colored state. The Blue solid (−) line represents the radiation pressure in the bleached state. The right vertical axis in red is the percent change between colored and bleached structures. The Red line represents the percent change in radiation pressure between the two colored and bleached states.

There is a small difference between the bleached state and the reflective state, separated by approximately 0.5 μN/m^2 with the colored state having the higher radiation pressure. With this small variation there is still a distinct peak in the relative change in radiation pressure at approximately 50 nm thickness of silicone. With the desire to see how the material's thicknesses interact to change the radiation pressure. A convert plot varying both layers of tungsten trioxide as well as the layer of silicone was created in Fig. 4.14.

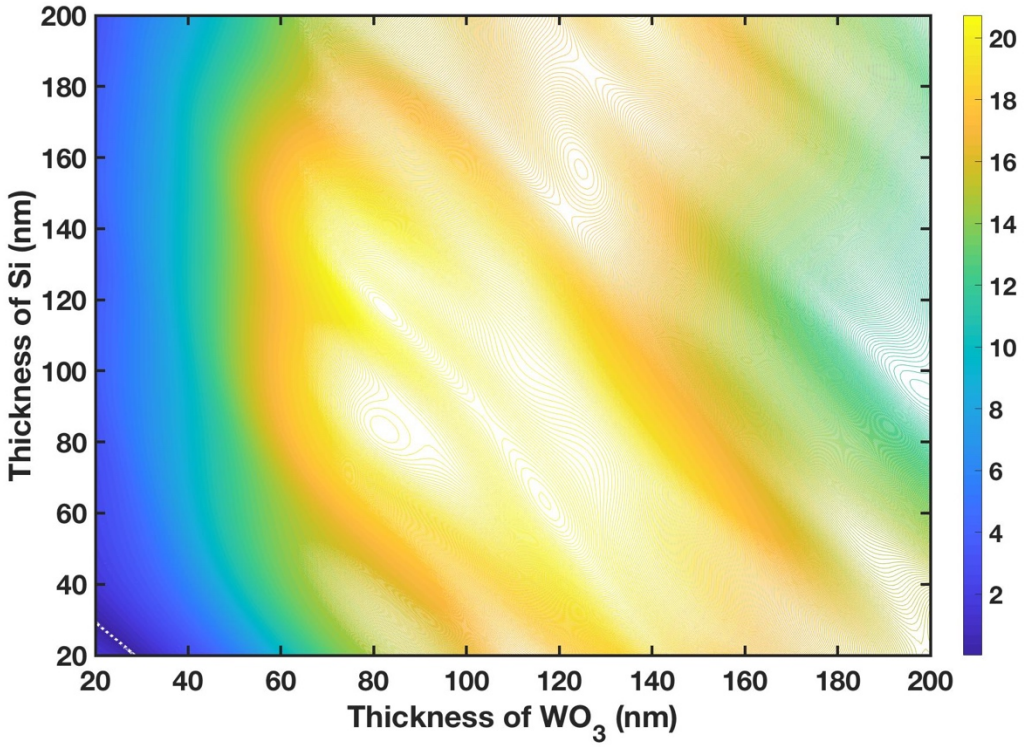

Figure 4.14: A top layer of tungsten trioxide, WO_3 varies from 20 nm to 200 nm, a middle layer of silicon, Si varies from 20 nm to 200 nm, and a bottom layer of WO_3 varies from 40 nm to 200 nm. A contour plot of WO_3 thickness, Si thickness, and percent relative change [%]. Vertical axis is the thickness of the silicone, Si, the horizontal axis is the thickness of tungsten trioxide, WO_3. The color scheme is percent relative change [%].

The results of the observations of the contour plot in Fig. 4.14 show that the best results are found from a moderate thickness in both the silicone and tungsten trioxide layers. More specifically at between 70 to 130 nm of the tungsten trioxide layer and between 60 to 120 nm of the silicone layer we see a large peak. This peak is above 20% relative change in radiation pressure shown in bright yellow. Although this figure reveals a great deal about the improvements that can be made it also opens the door for more research and optimization, further enhancing the modulation and radiation pressure.

Looking at the structures explored here it is very apparent that the third and latest iteration has the most promise for space applications. A 20% variation with a 5 $\mu N / m^2$ change between them has potential to be useful in space applications. Furthermore, this structure has the promise of being further optimized by adding an antireflective coating and further optimizing the thicknesses of each component.

CHAPTER 5

CONCLUSION & FUTURE WORK

This thesis explorer of the potential of tungsten trioxide (WO_3) on optical force modulation. The hope would be that someday this could be utilized to steer a solar sail across the planetary system and beyond.

Throughout this thesis four structures for modulating radiation pressure were explored. Two of these were opaque structures, and the remaining two were semitransparent. The opaque two-layer structure made of tungsten trioxide film on aluminum substrate (WO_3/Al) was analyzed and found to have a 26% relative change in radiation pressure with a WO_3 thickness of 200 nm. An opaque three-layer structure made of tungsten trioxide film on an undoped silicon layer on aluminum substrate (WO_3/Si/Al) was also explored, and it was found to have a 25% relative change in radiation pressure with 180 nm WO_3 and 20 nm Si. While the three-layer structure (WO_3/Si/Al) firms a Fábry Perot resonance cavity with enhanced absorption, it has comparable performance in radiation pressure modulation with the simpler two-layer structure (WO_3/Al). Besides, a two-layer semitransparent structure, made of tungsten trioxide film on silicone substrate (WO_3/Si), and was found to have an 8% change in radiation pressure with 200 nm WO_3 and 50 nm Si. A semitransparent three-layer structure, made of tungsten trioxide film on a silicone layer on tungsten trioxide (WO_3/Si/WO_3), was explored, which had a relative change in radiation pressure of 20% with 85 nm thickness for both the WO_3 layers and 90 nm Si. All four of the aforementioned structures were analyzed over the spectral range between 0.4 to 1.6 μm, which covers approximately 80% of the solar spectrum energy. Reflectance is twice as important as absorption in radiation pressure. It appears opaque surfaces are more advantageous

switching between reflection and absorption, than what is seen in the semitransparent structures which are switching between absorption and transmission.

Three of these support structures, WO_3/Al, WO_3/Si/Al and WO_3/Si/WO_3 showed an optical force modulation of 1.4, 1.34, and 0.65 $\mu N/m^{2.}$ Each of these exceeds the 7.8% relative change in radiation pressure with a change of 0.11 $\mu N/m^2$ found on the IKAROS, a Japanese JAXA mission to test whether modulating radiation pressure could be used for attitude control [2]. Studies since the launch of IKAROS have shown improving a greater percent change in radiation pressure up to 53%. This was done with liquid crystals with a change in radiation pressure of 0.5 $\mu N/m^2$ [5]. This allows the confident conclusion that WO_3/Al, WO_3/Si/Al and WO_3/Si/WO_3 show great promise for attitude control in future space missions, and may outperform the IKAROS mission.

The opaque structures in particular have proven to have the most promise going forward. For this reason, the structures WO_3/Al and WO_3/Si/Al are hoped to be studied further. Theoretically by the addition of the conducting layers that cause the tungsten trioxide to change from bleached to colored states. These layers would include a transparent electrical conductor layer, and an ion conductor layer in addition to the active layer of WO_3. It is also hoped to explore these structures experimentally. Both of the structures begin with a simple opaque aluminum wafer which would use an electron beam evaporation to add the layer of WO_3. The Si layer would be added using chemicals for deposition. With additional electrical current across the tungsten trioxide measurements will be taken both in the bleached and colored states. This thesis theoretically shows that tungsten trioxide (WO_3) has great promise for the solar sail allowing propulsion and attitude control of spacecraft, and ultimately the exploit with no fuel to the edges of the solar system and beyond.

REFERENCES

[1] P. Helfenstein, P. C. Thomas, and J. Veverka, "Evidence from Voyager II photometry for early resurfacing of Umbriel," *Nature*, 1989, doi: 10.1038/338324a0.

[2] R. Funase *et al.*, "On-orbit verification of fuel-free attitude control system for spinning solar sail utilizing solar radiation pressure," *Adv. Sp. Res.*, vol. 48, no. 11, pp. 1740–1746, 2011, doi: 10.1016/j.asr.2011.02.022.

[3] S. Taylor and L. Wang, "Vanadium dioxide-based variable reflectivity radiation coatings for optical propulsion applications," *Proc. Int. Astronaut. Congr. IAC*, no. September, pp. 26–30, 2016.

[4] L. P. Wang, S. Basu, and Z. M. Zhang, "Direct and indirect methods for calculating thermal emission from layered structures with nonuniform temperatures," *J. Heat Transfer*, vol. 133, no. 7, pp. 1–7, 2011, doi: 10.1115/1.4003543.

[5] D. Ma, J. Murray, and J. N. Munday, "Controllable Propulsion by Light: Steering a Solar Sail via Tunable Radiation Pressure," *Adv. Opt. Mater.*, vol. 5, no. 4, pp. 1–6, 2017, doi: 10.1002/adom.201600668.

[6] S. Taylor, Y. Yang, and L. Wang, "Vanadium dioxide based Fabry-Perot emitter for dynamic radiative cooling applications," *J. Quant. Spectrosc. Radiat. Transf.*, 2017, doi: 10.1016/j.jqsrt.2017.01.014.

[7] S. H. Lee *et al.*, "Crystalline WO3 nanoparticles for highly improved electrochromic applications," *Adv. Mater.*, vol. 18, no. 6, pp. 763–766, 2006, doi: 10.1002/adma.200501953.

[8] A. S. Barker, H. W. Verleur, and H. J. Guggenheim, "Infrared optical properties of vanadium dioxide above and below the transition temperature," *Phys. Rev. Lett.*, 1966, doi: 10.1103/PhysRevLett.17.1286.

[9] H. W. Verleur, A. S. Barker, and C. N. Berglund, "Optical properties of VO2 between 0.25 and 5 eV," *Rev. Mod. Phys.*, 1968, doi: 10.1103/RevModPhys.40.737.

[10] V. S. Braga, F. A. C. Garcia, J. A. Dias, and S. C. L. Dias, "Phase transition in niobium pentoxide supported on silica-alumina," *J. Therm. Anal. Calorim.*, 2008, doi: 10.1007/s10973-006-8325-4.

[11] F. A. Chudnovskii, L. L. Odynets, A. L. Pergament, and G. B. Stefanovich, "Electroforming and switching in oxides of transition metals: The role of metal-insulator transition in the switching mechanism," *J. Solid State Chem.*, 1996, doi: 10.1006/jssc.1996.0087.

[12] F. P. Emmenegger and M. L. A. Robinson, "Preparation and dielectric properties of niobium pentoxide crystals," *J. Phys. Chem. Solids*, 1968, doi: 10.1016/0022-3697(68)90109-1.

[13] S. Ulrich, C. Szyszko, S. Jung, and M. Vergöhl, "Electrochromic properties of mixed oxides based on titanium and niobium for smart window applications," *Surf. Coatings Technol.*, 2017, doi: 10.1016/j.surfcoat.2016.11.078.

[14] E. Pehlivan, K. Koc, F. Z. Tepehan, and G. G. Tepehan, "Structural, optical and electrochromic properties of tantalum pentoxide-doped niobium pentoxide thin films," *J. Sol-Gel Sci. Technol.*, 2016, doi: 10.1007/s10971-015-3841-y.

[15] "Refractive index of Nb2O5 (Niobium pentoxide) - Lemarchand." https://refractiveindex.info/?shelf=main&book=Nb2O5&page=Lemarchand (accessed Apr. 12, 2020).

[16] C.-C. Jaing *et al.*, "Optical constants of electrochromic films and contrast ratio of reflective electrochromic devices," *Appl. Opt.*, vol. 53, no. 4, p. A154, 2014, doi: 10.1364/ao.53.00a154.

[17] C. ViolBarbosa *et al.*, "Transparent conducting oxide induced by liquid electrolyte gating," *Proc. Natl. Acad. Sci. U. S. A.*, vol. 113, no. 40, pp. 11148–11151, 2016, doi: 10.1073/pnas.1611745113.

[18] D. H. Lowndes, D. B. Geohegan, A. A. Puretzky, D. P. Norton, and C. M. Rouleau, "Synthesis of novel thin-film materials by pulsed laser deposition," *Science (80-.).*, 1996, doi: 10.1126/science.273.5277.898.

[19] A. Piccolo and F. Simone, *Performance requirements for electrochromic smart window*, vol. 3. Elsevier, 2015.

[20] A. Piccolo and F. Simone, "Effect of switchable glazing on discomfort glare from windows," *Build. Environ.*, vol. 44, no. 6, pp. 1171–1180, 2009, doi: 10.1016/j.buildenv.2008.08.013.

[21] M. F. Modest, *Radiative Heat Transfer*. 2013.

[22] E. D. Palik, *Handbook of optical constants of solids*. 2012.

[23] F. G. Della Corte, M. E. Montefusco, L. Moretti, I. Rendina, and G. Cocorullo, “Temperature dependence analysis of the thermo-optic effect in silicon by single and double oscillator models,” *J. Appl. Phys.*, vol. 88, no. 12, pp. 7115–7119, 2000, doi: 10.1063/1.1328062.